

M. M. Connell

**NEURAL NETWORK APPROACH TO EVENT LOCATION  
WITH AN ANGER CAMERA  
FOR GAMMA RAY ASTRONOMY**

**BY**

**KENT REINHARD**  
B.S., University of Nebraska, 1985

**THESIS**

Submitted to the University of New Hampshire  
in Partial Fulfillment of  
the Requirements for the Degree of

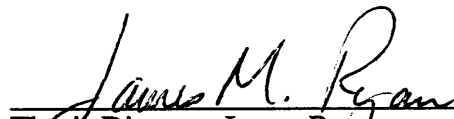
Master of Science


in

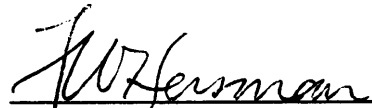
Physics

September, 1989

This thesis has been examined and approved.

  
\_\_\_\_\_  
Thesis Director, James Ryan  
Research Associate Professor of Physics

  
\_\_\_\_\_  
David Forrest  
Research Associate Professor of Physics

  
\_\_\_\_\_  
William Hersman  
Associate Professor of Physics

7/24/89  
Date

*This thesis is dedicated to my wife and family  
who provided me with constant encouragement.*

## **ACKNOWLEDGEMENTS**

I wish to express deep appreciation to my thesis advisor Research Professor James M. Ryan for his encouragement and guidance throughout this project. I would also like to thank all the people of the COMPTTEL group at the University of New Hampshire for their support, wonderful times in the hallways and for providing the terrific work environment. I would also like to thank the other faculty members and staff of the Physics Department for giving me the opportunity to study and work at the University of New Hampshire.

## LIST OF FIGURES

Figure 1.1	Gamma Ray Observatory.....	1
Figure 1.2	Compton Telescope.....	2
Figure 1.3	Compton Scattering Process.....	4
Figure 2.1	Regions of Gamma Ray Interaction.....	8
Figure 2.2	Bar Scintillation.....	10
Figure 2.3	Bar Scintillation.....	10
Figure 2.4	Bar Scintillation.....	11
Figure 3.1	Anger Camera.....	14
Figure 3.2	COMPTEL.....	15
Figure 3.3	D1 Platform.....	16
Figure 3.4	D1 Module.....	17
Figure 3.5	D2 Platform.....	18
Figure 3.6	D2 Module.....	18
Figure 4.1	Collimator.....	21
Figure 4.2	Transport Structure.....	22
Figure 4.3	D1 Module Mapping Run Locations.....	23
Figure 4.4	PMT Fluctuations.....	25
Figure 6.1	SM II Resolution Results.....	36
Figure 7.1	PMT Scaling Table.....	38
Figure 7.2	Neural Network Architecture.....	40
Figure 8.1	Generalization Parameter.....	43
Figure 8.2	Resolution and Location Speed.....	44
Figure 8.3	Beta Parameter.....	45
Figure 8.4	PMT Scaling Parameter.....	46

Figure 8.5	Neural Network Learning Curves.....	48
Figure 8.6	Quarter Module Resolution Contours.....	49
Figure 8.7	Energy Resolution.....	50
Figure 8.8	Event Location Speed.....	51
Figure 8.9	Full Module Resolution Contours.....	52
Figure 8.10	Module Resolution Area.....	53
Figure 8.11	Single Source File Event Location Contours.....	54
Figure 8.12	Background Flood Test Contours.....	56
Figure 8.13	Edge Source Files Event Location Contours.....	57

## **ABSTRACT**

### **NEURAL NETWORK APPROACH TO EVENT LOCATION WITH AN ANGER CAMERA FOR GAMMA RAY ASTRONOMY**

by

**Kent Reinhard**  
University of New Hampshire, September, 1989

COMPTEL is an imaging Compton telescope on the Gamma Ray Observatory. The telescope uses a two detector array for imaging and is sensitive to gamma rays in the energy range of .8 to 30 MeV. The imaging process is dependent on gamma ray energy deposits and the location of the gamma ray scattering within each of the detector arrays.

A mapping relationship between the photomultiplier space and physical space of the detector is used to determine an event's spatial location. An event location algorithm is used to find an event's location using this relationship.

Limitations with a chi square search algorithm have lead to the development of a new event location algorithm using a neural network. The learning of the neural network is similar to the trial and error learning process of the brain. The neural network adjusts a set of weights which are summed to produce the location of an event based upon the response of the detector. Requirements that the neural network must meet include achievement of the same spatial resolution of earlier tests and improvement of event location speed. Early development of the neural network demonstrated that it could locate events on a limited distribution of points and events.

Presented in this paper is the application of the neural network as an event location algorithm for an entire detector array. Also included is a description of the mapping process, the architecture of the neural network, and the performance of its event location

capabilities. We find that the neural network approach does in fact yield equally good RMS resolution values of 2.3 cm. Comparison of the event location speed with earlier algorithms shows an improvement by a factor of 15 with the neural network.



## TABLE OF CONTENTS

DEDICATION.....	iii
ACKNOWLEDGEMENTS.....	iv
LIST OF FIGURES.....	v
ABSTRACT.....	vii

CHAPTER	PAGE
1. INTRODUCTION.....	1
Compton Telescope.....	2
Event Location for Directional Imaging.....	3
Event Location Speed.....	5
2. PHYSICS OF SCINTILLATION.....	7
Major Types of Interaction.....	7
Scintillation Techniques.....	8
Photomultiplier Space.....	9
3. PREVIOUS WORK.....	13
Medical Anger Camera.....	13
Science Model II.....	15
COMPTEL.....	15
D1 Detector Platform.....	16
D2 Detector Platform.....	17
4. DATA.....	20
Mapping Procedure.....	20
Hardware Description.....	20
Grid System.....	21

	Applied Corrections.....	24
5.	THREE DIMENSIONAL DESCRIPTION.....	27
	Principle Component Analysis.....	27
	COMPTEL Applications.....	29
6.	CHI SQUARE MINIMIZATION.....	33
7.	NEURAL NETWORK.....	37
	Architecture.....	37
	Learning.....	39
	Testing.....	41
8.	TEST RESULTS.....	42
	Parameter Test.....	42
	Quarter Module Test.....	47
	Full Module Test.....	51
	Background Flood Test.....	55
9.	DISCUSSION.....	58
	Quarter Module Test.....	59
	Full Module Test.....	60
	Maximum Resolution.....	60
	Effects on COMPTEL Resolution.....	61
	Further Development.....	62
	Integration of Other Quantities.....	62
	REFERENCES.....	63

## CHAPTER 1

### INTRODUCTION

When people hear the term astronomy they often think of vivid pictures produced by telescopes using visible light. During the last few decades, however, astronomy has outgrown the boundaries of the visible spectrum. Modern astronomy uses the entire range of the electromagnetic spectrum, from radiowaves to gamma rays, to build a better picture of the structure and workings of the universe.

Since the introduction of satellites, the field of astronomy which involves research with high energy photons has expanded. Some of the latest contributions to the field of gamma ray astronomy will come from NASA's new satellite platform, Gamma Ray Observatory (GRO), shown in Figure 1.1.

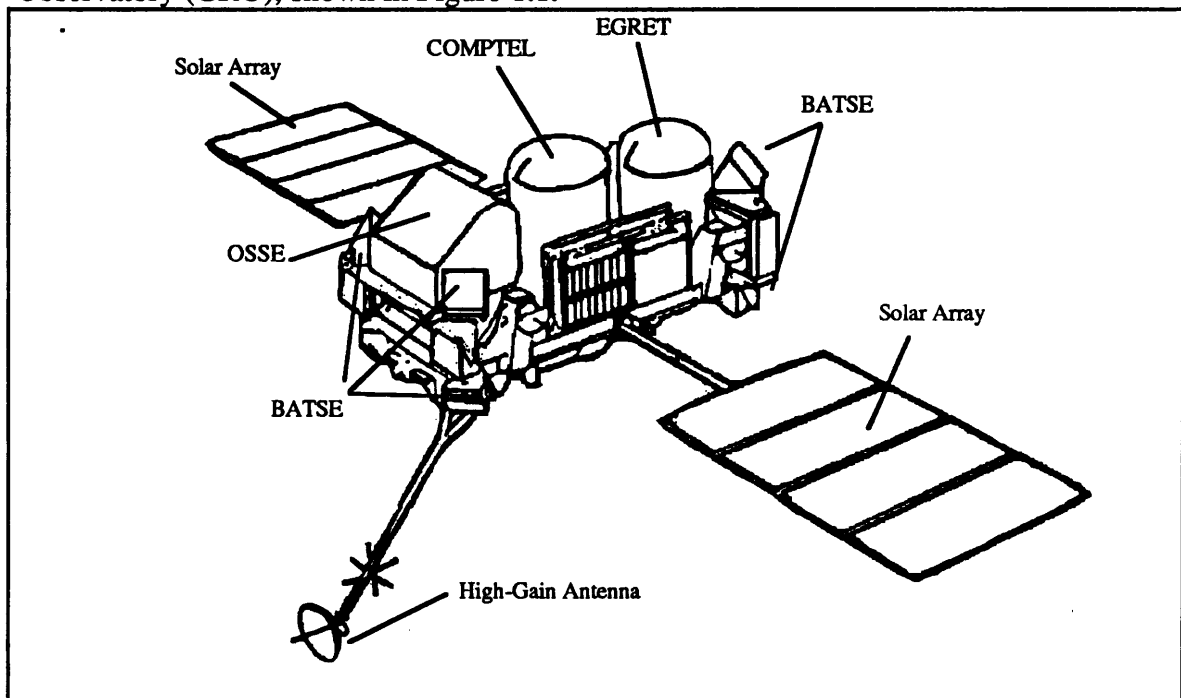


Figure 1.1 The Gamma Ray Observatory (GRO) will measure a large range of the gamma ray spectrum. This satellite houses four instruments that are sensitive at different energy ranges. The instruments are the Oriented Scintillation Spectrometer Experiment (on the left), the Burst and Transient Source Experiment (on the eight corners), the Compton Telescope (in the center), and the Energetic Gamma Ray Experiment Telescope (on the right) [NASA 1988].

GRO will house four different experiments designed to study a large range of the gamma ray spectrum from energies of .02 MeV to 20 GeV. Once GRO is launched from the space shuttle, it will operate at an altitude of 450 kilometers for approximately two years. The four instruments on board GRO are the Compton Telescope (COMPTEL), the Oriented Scintillation Spectrometer Experiment (OSSE), the Burst and Transient Source Experiment (BATSE), and the Energetic Gamma Ray Experiment Telescope (EGRET) [Kniffen 1988].

### Compton Telescope

At the University of New Hampshire (UNH) work is being conducted on the operation and construction of the COMPTEL experiment. COMPTEL is designed to detect gamma rays in the energy range of .8 to 30 MeV by using the combination of Compton scattering and the Photoelectric effect [Schönfelder 1984].

COMPTEL consists of an upper detector array know as D1 and a lower detector array D2 as shown in Figure 1.2.

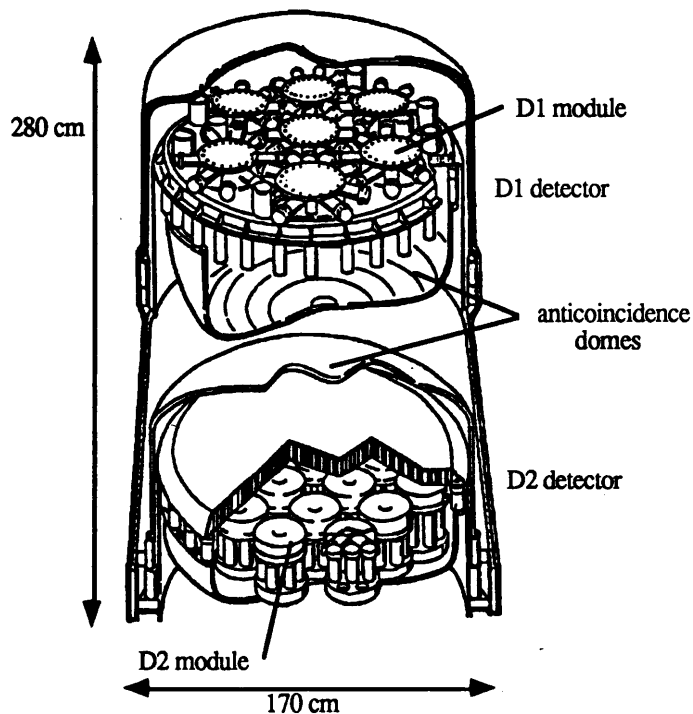


Figure 1.2 The Compton Telescope (COMPTEL) aboard (GRO). The telescope is sensitive to gamma rays in the energy range of .8 to 30 MeVs. It uses a combination of two detectors to image the direction of gamma rays [Kniffen 1988].

The D1 array consists of seven modules filled with a liquid scintillator ideal for Compton scattering of gamma rays. Each module is viewed by eight photomultiplier tubes (PMTs) and uses the Anger camera principle for event location inside the module. D2 is composed of fourteen scintillation crystal detectors which work on the photoelectric principle, Compton scattering, and pair production for gamma ray detection. Each crystal, or module, is viewed by seven PMTs and also uses the Anger camera principle for event location.

### **Event Location for Directional Imaging**

The mechanism of the Compton Telescope works when an incident gamma ray undergoes Compton scattering in the D1 detector, imparting part of its energy to a bound electron in the liquid. The scattered photon can then continue on to the lower D2 detector where it may be absorbed by a crystal and deposit its remaining energy.

The energy deposited in the two detectors determines the scatter angle between the incident direction and scatter direction of the photon as shown in Figure 1.3. The scatter angle is given by:

$$\cos(\theta) = 1 - m_0c^2 \left( \frac{1}{E_1} - \frac{1}{E_1 + E_2} \right)$$

where  $m_0$  is the rest mass of the electron, and  $E_1$  and  $E_2$  is the energy deposited in the D1 and D2 detectors respectively. The scatter direction is determined from the interaction locations within the detectors. The direction of the incident photon is determined from the scatter angle and scatter direction. These two quantities will form an event cone with an edge called an event circle as shown in Figure 1.3. If there are many photons coming from a source the location of that source is determined by looking at the intersection of the many event circles produced.

The need for event location and energy resolution inside the detector is critical in determining the overall resolution of the detector. Earlier models of the Compton

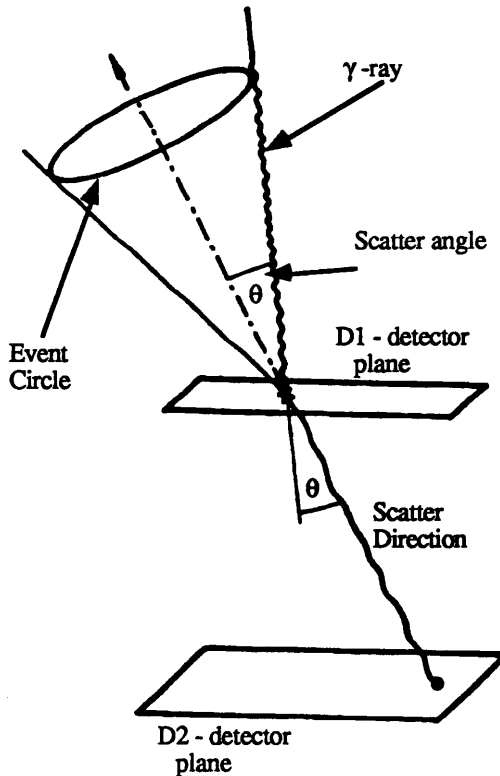


Figure 1.3 The basic Compton scattering process of COMPTEL. The incident gamma ray is scattered in one of the D1 modules and then one of the D2 modules. The event's location in the two detectors defines the scatter direction and the energy deposited in both detectors determines the scatter angle ( $\theta$ ) [Schönfelder 1982].

telescopes worked on basically the same principle, but they did not have any spatial resolution inside the detectors. The limiting factor for these earlier models was the inability to determine the scatter direction more accurately than the detector size itself. This inability to locate the event interaction inside the detectors contributed largely to the overall poor resolution of these detectors.

With the use of the Anger camera principle in COMPTEL, the projected resolution will be a factor ten better than some of the older Compton telescopes. The main reason for this increase is the use of the event location inside the detectors providing a much better estimate of the scatter direction.

Part of the development work at UNH involves the production of algorithms and software systems which will perform event location and determine energy resolution within the detectors of COMPTEL. One of the most recent developments in the area of location

algorithms focuses on the integration of a neural network system as the major event location algorithm.

### **Event Location Speed**

In addition to event location, another problem facing COMPTEL is the computer time required for the processing of an event. COMPTEL will transmit approximately five astrophysically interesting events per second. Early tests using old algorithms showed that it would take approximately five seconds of CPU time to process each event. The speed of a more recent chi square minimization algorithm has been improved so that its performance will process events, with energies of 1 MeV, at the rate of 70 events per second of CPU time. Estimates using this higher rate indicate that it will take about 4 CPU months [Simpson 1987] to process the entire COMPTEL volume of data. These values are for astrophysical events only and do not include all the other possible events. It is estimated that the present algorithm will take up about 25 percent of the computer resources available for event processing alone. We will show that the neural net algorithm now being tested will improve event location speed, thus reducing the backlog of event processing expected.

The initial use of a neural network for event location consisted of learning and testing over a small and limited distribution of points containing a limited number of events [Simpson 1987]. The work presented in this paper extends this initial work of the neural network by conducting tests using the complete set of mapping points that cover the entire area of a D1 module. It attempts to establish the advantages the neural network has over the current algorithms.

The physics of scintillation is described in Chapter 2 along with the use of the PMT signals to describe an event location. Chapter 3 covers the physical description of the detector and early work which introduced the Anger Camera technique to event location. In Chapter 4 is a discussion of the data which is used in the testing of the neural network. Also included is a discussion of the corrections required for this data in order for it to be used in the mapping process. Chapter 5 discusses how Principle Component Analysis

(PCA) can be used to extract information about event location from the PMT signals. Also covered is the formation of the Correlation matrix and its eigenvectors and eigenvalues which are used in the formation of new PMT space. Results from the early science model and chi squared minimization algorithm are covered in Chapter 6. Background of the neural network is given in Chapter 7 along with a description of the structure and operation of the neural network. The results of the testing of the neural network on a D1 module are covered in Chapter 8.



## CHAPTER 2

### PHYSICS OF SCINTILLATION

The interaction of gamma rays with material is important because through this interaction that they are detectable. It is at the quantum level that a gamma ray produces a charged particle and it is through these secondary particles that the information of the gamma ray is made available.

#### Major Types of Interaction

The three major interactions for gamma rays are Compton scattering, photoelectric effect, and pair production process.

Compton scattering is the interaction of a gamma ray and a bound electron. The gamma ray scatters off a bound electron, imparting some of its energy to the electron thus ionizing the atom. The energy range in which Compton scattering is effective is between the .5 and 10 MeV region.

A gamma ray could also interact with material by the photoelectric effect. This process, too, occurs between a gamma ray and a bound electron. In the interaction, the photon imparts all of its energy to the electron. The chance of the photoelectric effect occurring is related to the atomic number ( $Z$ ) of the material and the energy of the photon. The photoelectric effect is most effective for high  $Z$  material up to the energy of about 1 MeV after which Compton scattering dominates.

Above the 10 MeV range, the pair production process dominates for high  $Z$  material. Pair production is an interaction of a gamma ray and an atomic nucleus. From this interaction, an electron and positron are produced as the photon is annihilated. The energy from the photon is for the most part in the positron-electron pair with little energy being deposited in the nucleus. Figure 2.1 shows the energy regions versus the atomic number where the three major photon interactions dominate.

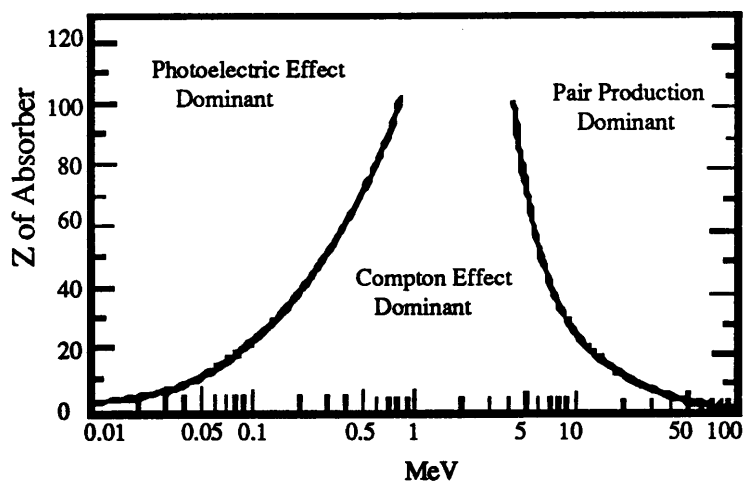


Figure 2.1 Relative importance of the major types of gamma ray interactions. The lines shown where the two neighboring effects are just equal [Evans 1955].

In the energy range of 0.5 to 3.0 MeV the range of the scattered electron is given

by:

$$R_0(\text{g/cm}^2) = 0.52E(\text{MeV}) - 0.09$$

where  $R_0$  is the maximum range of the electron with and energy  $E$  [Evans 1955].

### Scintillation Techniques

Scintillation is an indirect way of detecting and measuring gamma rays. A scintillation detector's operation depends primarily on gamma rays losing energy through ionization of the detector's material. After ionization, the scattered electron converts its energy into visible photons which are detected by photomultiplier tubes viewing the scintillation.

The main component of a scintillation detector is a large volume of homogeneous material in which the gamma rays can interact. The important property of the material is that it convert the energy lost by the gamma ray to visible photons, and the number of visible photons produced be proportional to the energy deposited by the gamma ray. Ideally, the material should be able to produce a large number of visible photons for a small amount of deposited energy. The number of photons produced determines the energy resolution of the detector system. The material must also be transparent to the type of

visible photons produced so that it can be monitored by light measuring devices outside the scintillation material.

In most cases it is photomultiplier tubes (PMTs) which monitor the scintillation material and measure the intensity of the photon flux produced from a scintillation. Each PMT produces an electronic pulse proportional to the visible photon flux entering the PMT. Using the range of the output signals of the PMTs, a spectrum can be produced which is a measure of the energy lost from gamma ray interaction in the detector material.

### **Photomultiplier Space**

The photomultiplier output signals can also be used to determine where the gamma ray interaction occurred within the detector.

If more than one PMT is used to monitor the detector, each tube will receive a certain percentage of the photons produced by the scintillation. The location of the event inside the detector determines the strength of the PMT signals relative to one another. If an event takes place close to one of the PMTs, that PMT should receive most of the visible photons produced. The other PMTs will receive a smaller percentage of the remaining photons depending on their relative distance from the event. This set of PMT signals (amplitudes) form a PMT space which has N-dimensions where N is equal to the number of PMTs viewing the detector. For each physical location (x,y,z) in the detector there corresponds a point (p<sub>1</sub>,p<sub>2</sub>,...p<sub>N</sub>) in PMT space.

A simple way to describe the physics is to examine a hypothetical detector made up of a bar of scintillation material viewed by three photomultiplier tubes. The length, width and depth of the bar is described in physical space by a coordinate system x, y, and z, respectively. The physical location of an event in the bar is given by the vector:

$$\vec{S} = (x,y,z)$$

If an event happens in the middle and toward the top of the bar each PMT will view the event by the resulting photons (Figure 2.2). The PMT closest to the event, in this case

PMT 2, will receive the largest number of photons, resulting in the largest signal. PMT 1 and PMT 3 will receive equal but fewer numbers of photons producing smaller but equal signals. The event in PMT space is given by a vector of the form:

$$\vec{P}=(p_1,p_2,p_3)$$

with

$$p_2 > p_1 = p_3$$

where  $p_1$ ,  $p_2$  and  $p_3$  are the PMT signal pulses from PMT1, PMT2 and PMT3.

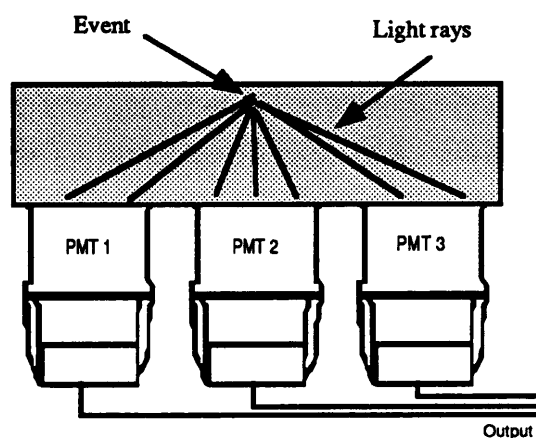


Figure 2.2

If a different event happens at the same depth in the bar but directly over PMT1, as shown in Figure 2.3, the physical coordinate  $z$  remains the same while  $x$  and  $y$  change.

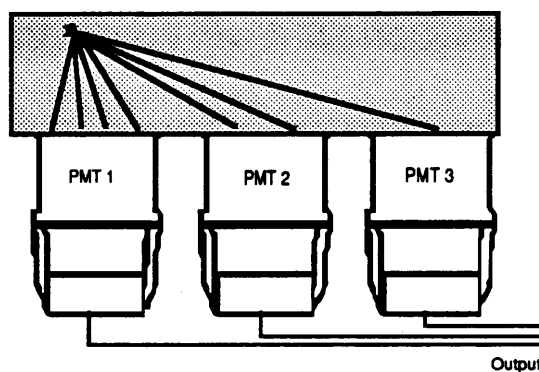


Figure 2.3

Because the event happens closer to PMT1, it receives most of the light. PMT2 is the next closest PMT and receives less than PMT1 but more than the more distant PMT3.

The vector in PMT space changes as does the physical space vector. The new PMT space vector has elements which are defined as:

$$p_1 > p_2 > p_3$$

The depth of an event within the detector can also be determined using the PMT signal. For example, an event that has the same x and y location as the first event, but is located deeper in the bar (different z location), is shown in Figure 2.4. The event occurs closer to PMT2 allowing it to receive even more events than it did in the earlier example.

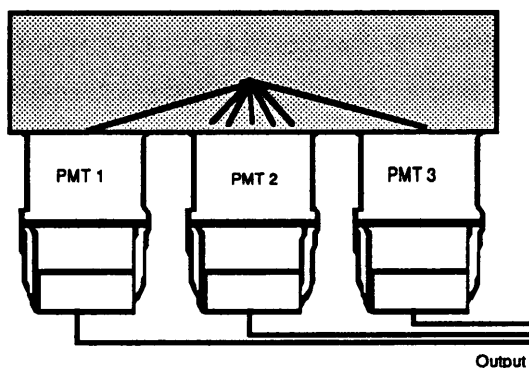


Figure 2.4

This leaves fewer photons for PMT1 and PMT3 to detect resulting in smaller signals from both. The new vector in PMT space resembles that of the event in the first example but the strengths of the signal will differ where:

$$p_2 \gg p_1 = p_3$$

The PMT space can be used to describe the physical location of an event in the detector if the relationship between the two are known. The mapping that gives the relationship between the two spaces is performed by radiating the detector at a known location and measuring the response of the PMTs. A description of this mapping process for the COMPTTEL detectors is discussed in Chapter 4.

location and measuring the response of the PMTs. A description of this mapping process for the COMPTEL detectors is discussed in Chapter 4.

## CHAPTER 3

### PREVIOUS WORK

#### Medical Anger Camera

Within the medical field, the need to measure the distribution of a radioactive tracer distribution within a subject lead to the development of a gamma ray camera. Early cameras employed techniques which took considerable time between the actual exposure and the final picture of the tracer distribution. A new camera was designed to produce a picture of the distribution of gamma rays but with a new and faster method that would cut down on the time between exposure and the production time of a final image.

Hal O. Anger developed the first such camera at the University of California, Berkeley [Anger 1958]. His device, called a scintillation camera, utilized a scintillation crystal viewed by several phototubes. The quick scintillation in the crystal and the conveyance of the scintillation by the phototubes produced an image immediately after the exposure.

The scintillation camera consisted of a large lead shield housing the scintillation crystal and seven phototubes (See Figure 3.1). One end of the camera had a pinhole aperture which allows gamma rays to enter and strike one side of the scintillation crystal, thereby focusing the gamma rays on the crystal in the pattern of the tracer source. Behind the crystal were several phototubes to detect the light from the scintillation and transform it into a usable signal.

The scintillation crystal consisted of thallium-activated sodium iodide material 4 inches in diameter and 0.25 inch thick. Behind the crystal were seven phototubes of 1.5 inch diameter. These phototubes measured light emitted from a scintillation. The amount of light received by each phototube depends on the distance of the event from the phototube, with the tube closest to the event receiving the most light. Attached to the output

of the phototubes is a location matrix circuit used to interpret the amplitudes produced from each of the phototubes. The matrix circuit adds and subtracts the amplitudes to produce three signals containing information about the event.

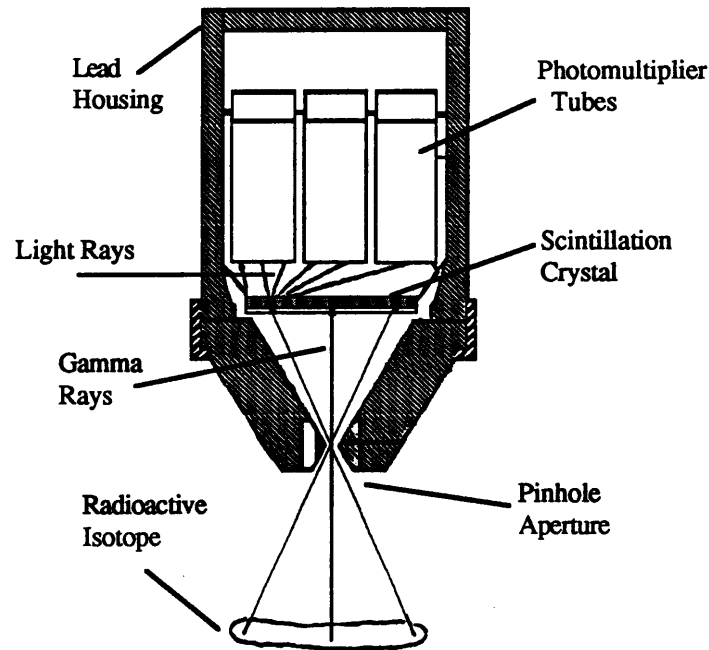


Figure 3.1 The original Anger Camera arrangement. The gamma rays are allowed to enter the camera through the pinhole aperture thus forming an image on the crystal. The gamma rays interact with the scintillation crystal producing light rays which the phototubes can detect. The signals from the tubes are used to produce an image of the gamma ray source [Anger 1958].

Two of the signals correspond to a x and y location of the event along the face of the crystal. The third signal is proportional to the sum of the amplitudes of the phototubes.

The sum signal is used to filter the type of events to be imaged. If the sum is between the values set by the controller, the location signal is transmitted to an oscilloscope. The location of the oscilloscope beam is positioned on an x and y grid system using the location signals from the matrix circuit. For each accepted scintillation event in the crystal, a flash will appear on the oscilloscope screen with a particular x and y value. The oscilloscope screen is photographed over a period of time allowing an image of the source to build up on the photographic film. This film could then be developed quickly thereby producing an image shortly after exposure.



Since it was first introduced by H.O. Anger, the technique of using phototubes to produce a spatial location within a scintillator has been used extensively in the fields of medicine and more recently astronomy. Detectors that use scintillation material viewed by several phototubes are called scintillation cameras or more accurately Anger Scintillation Cameras or Anger Cameras.

### Science Model II

During the development of COMPTEL three science prototypes have been built. One of these prototype models is Science Model 2 or SM-II. SM-II was built on the same principles and size as COMPTEL but with only one module in each of the D1 and D2 detectors. SM-II was extensively tested to determine the limitations of COMPTEL and to examine potential problems.

### COMPTEL

COMPTEL is a two detector array shown in Figure 3.2.

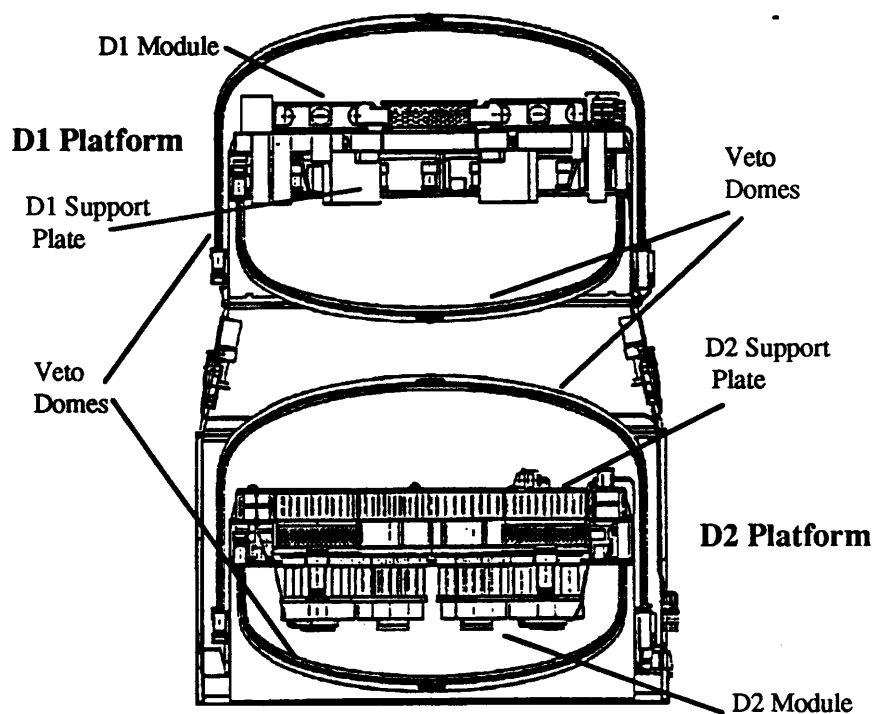


Figure 3.2 A side view of the Compton Telescope [Lichti 1982].

### D1 Detector Platform

The upper platform housed the D1 array, which consists of seven modules that lie in the plane of the platform. Module 1 is located at the exact center of the D1 platform, and is the center of the origin of the D1 detector coordinate system. The other six modules are located around this central module, with Module 2 lying along the negative x direction of the platform. The remaining modules are numbered in the counter-clockwise direction as shown in Figure 3.3.

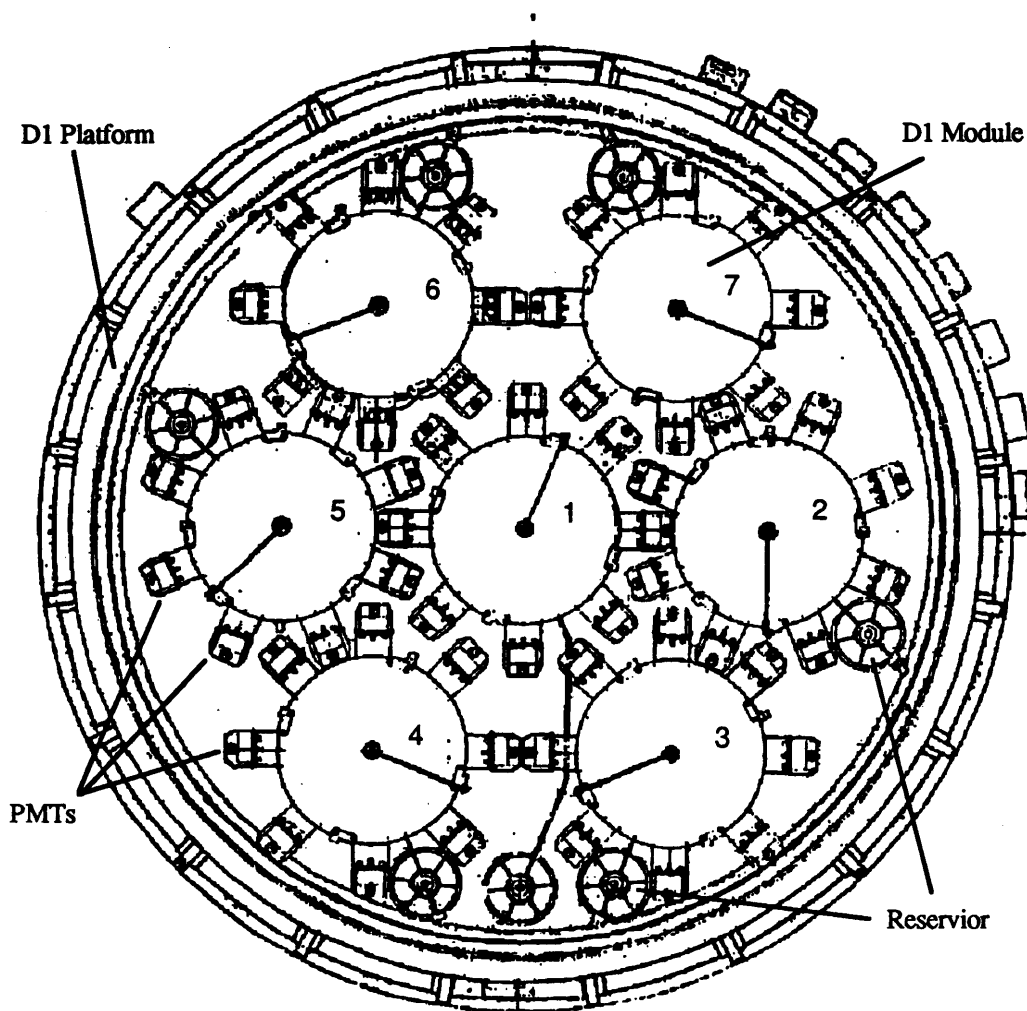


Figure 3.3 A top view of the D1 platform and the 7 modules [Zeckau 1982].

Each of the D1 modules (Figure 3.4) is a cylindrical chamber 28 cm in diameter and 8.5 cm deep. 5.5 liters of a organic scintillating liquid, NE213A, are used in each of the modules. Each module is viewed from the perimeter by eight PMTs (EMI 9755NA), and the event location uses the Anger Camera Principle. Each of the PMTs is assigned a number, 1 through 8, starting with the closest PMT which is clockwise (when viewed from the top) of the liquid reservoir.

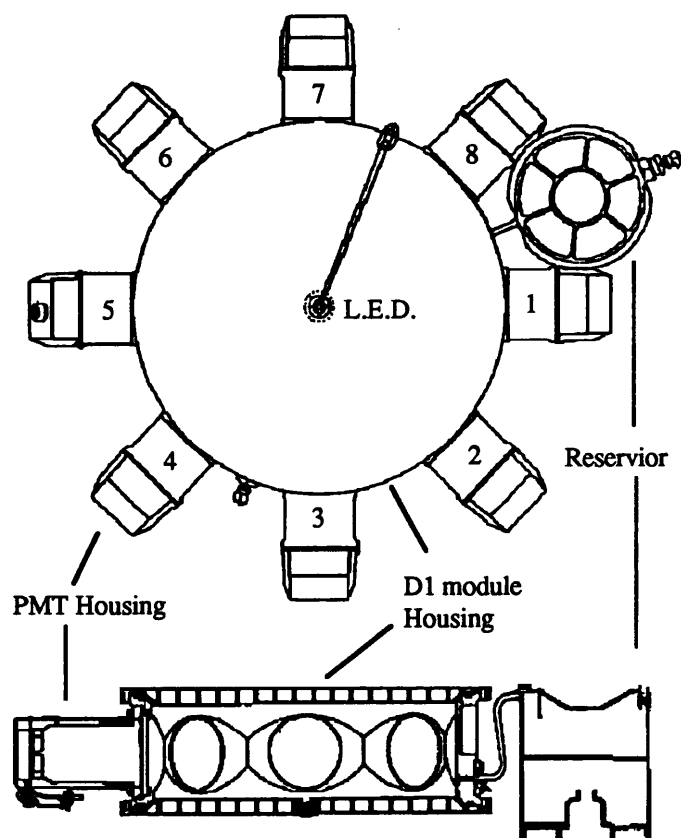


Figure 3.4 A top and side view of a D1 module [Lockwood 1984].

### **D2 Detector Platform**

The lower detector of COMPTTEL is the D2 detector. It is comprised of 14 modules housed below a support plate. Four of the modules are situated symmetrically about the origin and x and y axis of the D2 platform coordinate system. The remaining ten modules

are located outside of the four central modules. Figure 3.5 shows the arrangement of the D2 platform and the modules.

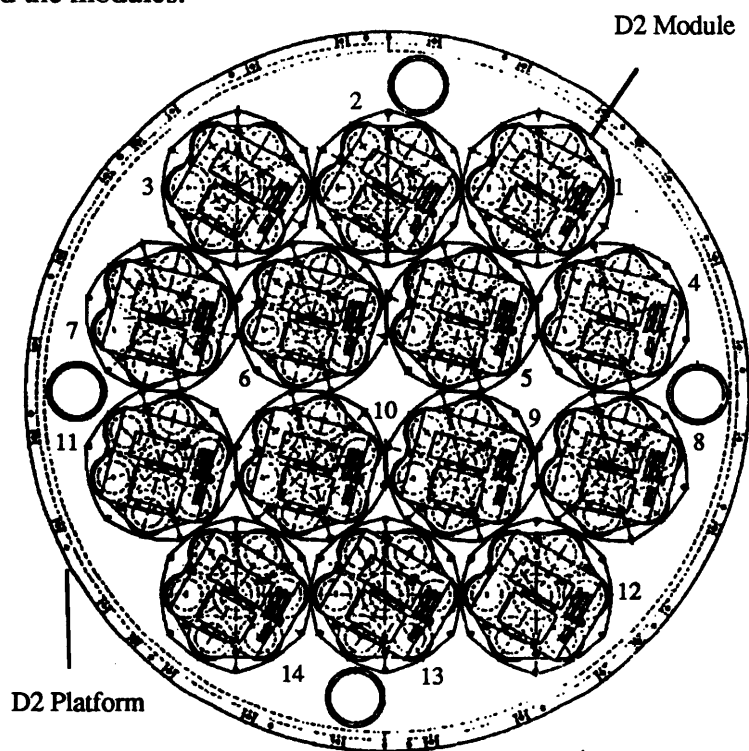


Figure 3.5 A bottom view of the D2 platform and the 14 module detectors [Lichti 1984].

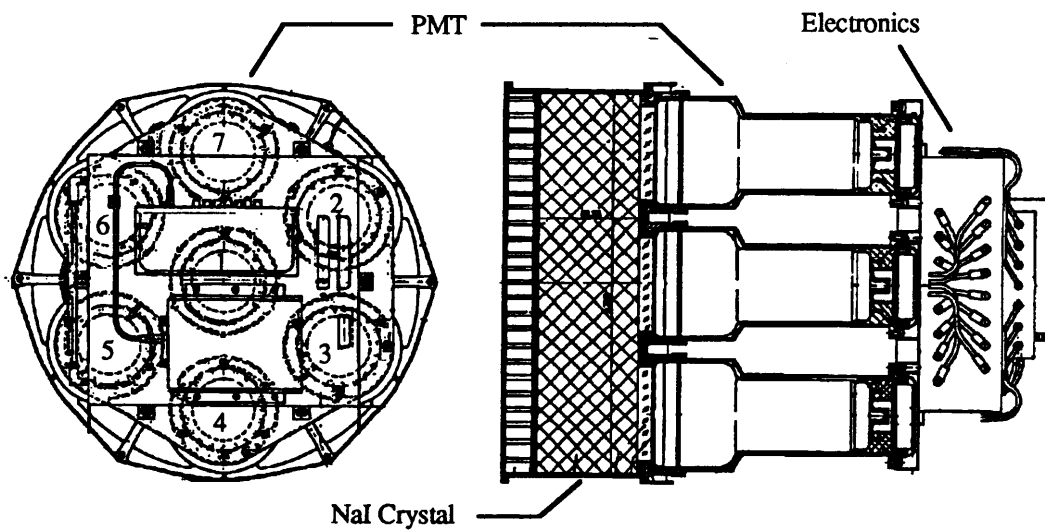


Figure 3.6 A side and bottom view of a D2 module [Lichti 1982].

Figure 3.6 shows the configuration of a D2 module. Each of the D2 modules is composed of a cylindrical Sodium Iodine (NaI (T1)) crystal 28.5 cm in diameter and 7.5 cm thick. Each crystal is viewed from the bottom (the side opposite the D1 detector) by seven PMTs (EMI 9754 NA). The PMTs are positioned with the number one PMT in the exact center of the back of the crystal. The number 2 PMT is the first PMT counter-clockwise from the LED and the others are numbered continuing in the counter-clockwise direction when viewed from the bottom.

## **CHAPTER 4**

### **DATA**

#### **Mapping Procedure**

The relationship between PMT space and physical 3-D space is found by using a mapping process that produces output vectors describing the same point in each of the two spaces. This mapping process consists of radiating a detector with a gamma ray beam at a known physical coordinate and monitoring the PMTs' response.

#### **Hardware Description**

The hardware used in this detector mapping consists of a lead collimator supported on a transport structure. The collimator is used to house the gamma ray source and position its beam at different locations above the detectors .

The collimator is a large lead casting, in a stainless steel housing, with a tungsten column as its axis. The collimator contains 216 kilograms of lead in a casing 350 mm long. The casing has a bell shape with an upper diameter of 200mm and a bottom diameter of 330 mm as shown in Figure 4.1. The column is used to hold the gamma ray source and alignment scope. The boroscope is used to visually verify the location of the collimator's center above the platform. A  $^{60}\text{Co}$  source of gamma rays is inserted 90 mm from the top of the tungsten column. From this location the lead collimator confines the gamma rays to a beam 10 mm in diameter perpendicular to the detector. The collimator is equipped with a 70 mm thick tungsten shutter on the underside of the bell housing. This shutter, in its closed position, is used to block the beam of gamma rays

The transport structure is a frame designed to fit along the edges of the platform and cause no obstruction of the detectors. Part of the frame consists of rails that lie along the coordinate axes and are used to guide and support the collimator 100 mm above each of the detectors. Additionally, the structure has two screw drives that position the collimator.

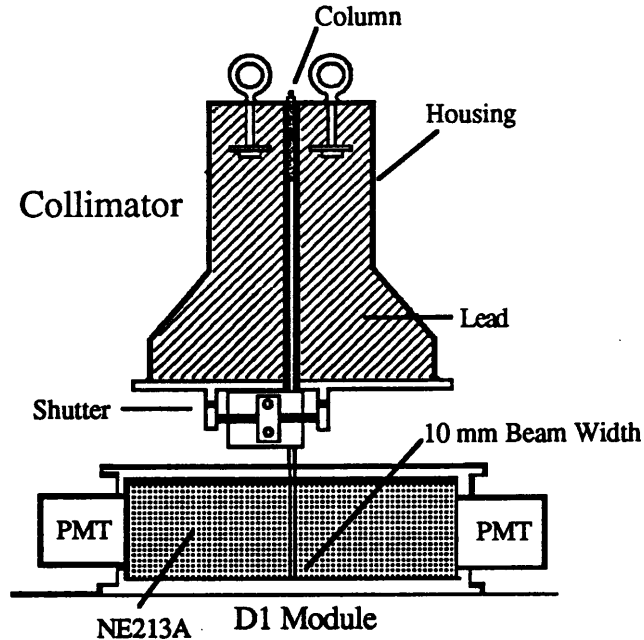


Figure 4.1 The lead collimator positioned over a D1 module [Deihl 1984, Lockwood 1984].

along the x and y directions. On the end of each screw drive shaft is an encoder which indicates the x or y position of the collimator. These encoders are wired directly to the computer where their readouts are recorded for each position of the mapping process. The transport structure is shown in Figure 4.2.

### Grid System

The grid system used to describe the beams location is an x and y coordinate system, with the origin located at one corner of the platform (Figure 4.2). All measurements taken during mapping are relative to that origin. Prior to the mapping procedure, a set of x and y coordinates were generated and used to position the collimator above each of the modules. The sets of coordinates used for each module consisted of approximately 900 different x and y values designed to position the collimator over the entire surface of the module.

At each of the predefined locations, the PMTs signals from the module directly below the collimator, and the x and y position are recorded on magnetic tape. Between 6,000 and 25,000 event signals are recorded at each of these locations. The entire set of

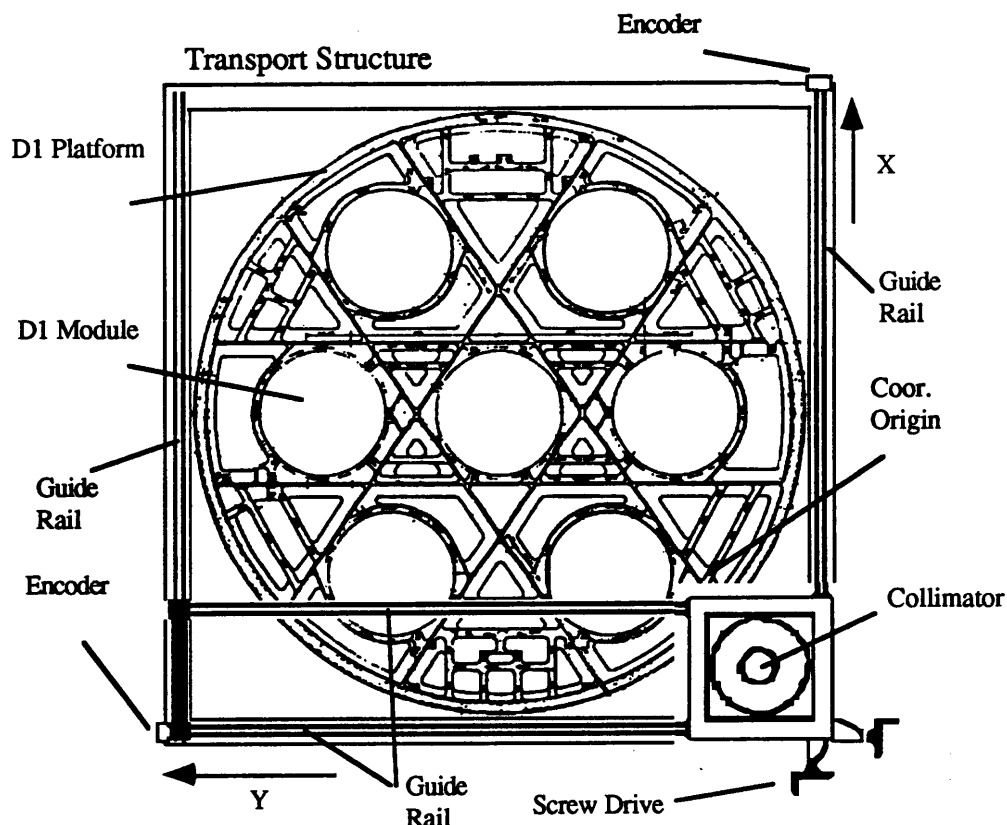


Figure 4.2 The transport structure is shown sitting on the D1 platform [Franz 1984, Lockwood 1984].

recorded events and the corresponding x-y coordinates is called a "mapping run". After every 25 runs the collimator is positioned at the center of the module being mapped. The readings from these "central" runs are used to monitor any changes that might occur in the detector system.

Early studies of SM-II indicated that in order to achieve the best results from module mapping, different types of runs would have to be conducted. The type of run would depend on the position of the collimator relative to the module.

In the time frame of the mapping procedure three different mapping passes were made over each of the detectors. Pass 1 covered most of the area of each module. Pass 2 was confined to only the areas in front of each of the PMTs and some central runs. Pass 3 covered the same area as Pass 1 but the locations are intermixed with the points of Pass 1. Figure 4.3 shows the location of the runs for one of the D1 module. The area of a module



that Pass 1 and Pass 3 covered is shown in Figure 4.3. Both Pass 1 and Pass 3 were conducted with runs that contained between 6,000 to 8,000 events per run. Pass 2 runs contain approximately 25,000 events per run file and were concentrated in the areas in front of the PMTs .

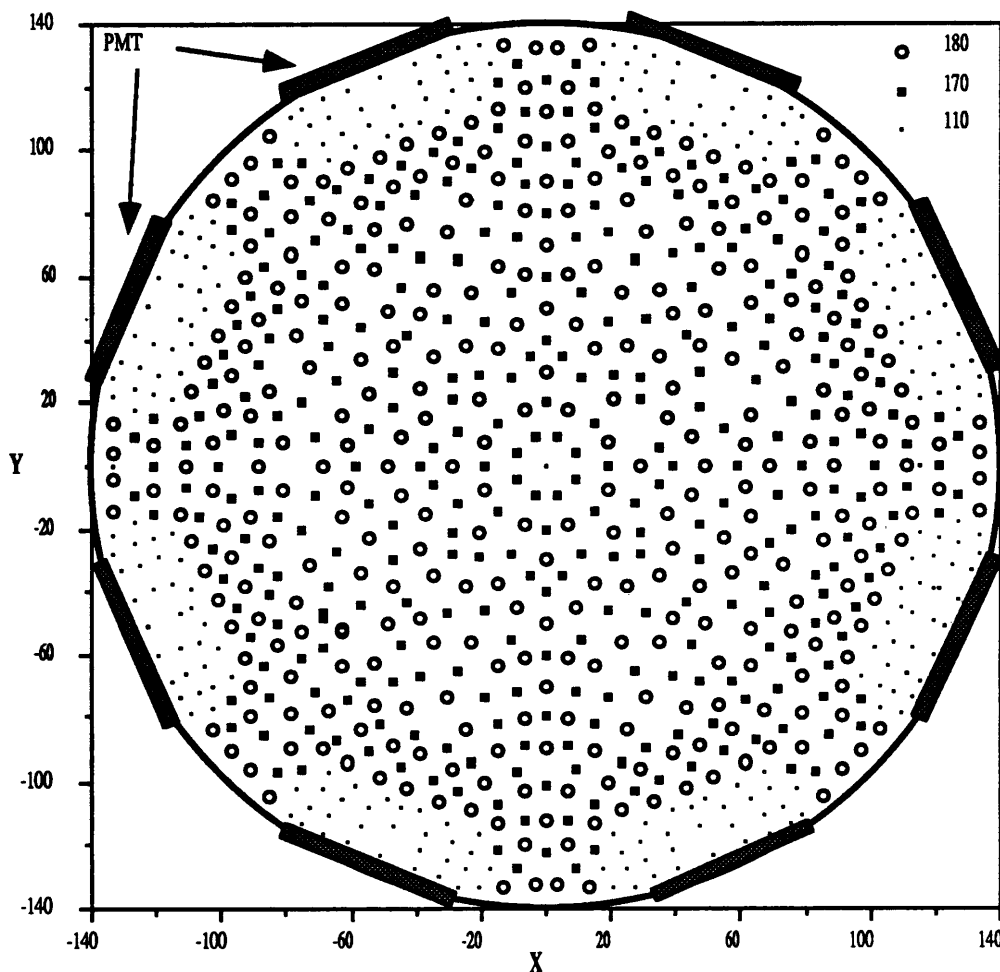


Figure 4.3 The location of the mapping runs for a D1 module. The mapping passes, Pass 1, Pass 2, and Pass 3 are represented by their threshold value 180, 110, and 170 respectively.

A major difference between the three passes, beside the times in which they were conducted and the different locations, is the physical threshold of the data. Threshold refers to the lower limit set on the pulse height analyzer which monitors the total output of the PMT signals or PMT Sum. The analyzer has a set of channels from 0 to 511 that the Sum of an event will fall between. If an event's sum is not above the threshold value, the

event is not accepted for recording. This threshold is used to select the energy range of accepted events, because the PMT Sum is directly related to the energy deposited by the incident photon. During most of the mapping, the more useful events would fall above channel 100 because the Compton edge for  $^{60}\text{Co}$  fell in channel 235. The thresholds that were used were 180, 110, and 170 for Pass 1, Pass 2 and Pass 3 respectively.

At selected locations, the threshold was changed to 0 meaning there was no limit on the PMT Sum thus allowing all events to be recorded. These runs are called "Open Window Runs" and consist of events of all energies.

### **Applied Corrections**

The next step in the mapping process is to correct the stored (raw data) runs. These corrections insure the proper production of a map between PMT and physical space. The corrections involve a series of tuning, calibration, and central run corrections designed to eliminate any fluctuations which might influence the final map.

The first set of corrections consist of the adjustment of the signals from each of the PMTs. The Analog-Electronic (AE) calibrations insure constant performance of each PMT over their expected input range. The AE corrections are determined by sending electronic pulser signals through the electronics and recording the output. These known pulser signals cover the input range of 0 to 360. The electronics output is plotted against the input signal. The line that best fits the distribution of points in the plot is used to determine the y intercept and slope. The intercepts and slopes for each PMT are stored in an array which is used in the correction software. This process is done for each PMT of every module.

The corrections are applied using correction software designed to work with the raw data. The AE corrections are applied to each event's signals by:

$$s_c = \frac{s_r - y_0}{M}$$

where  $s_r$  is the raw signal,  $y_0$  and  $M$  are the stored intercept and slope values, and  $s_c$  is the AE-corrected signal.

The next step in the correction process is to "tune" each of the of PMTs for a module. This tuning, or Gain Base Line Factor (GBLF), is designed to equalize the PMT's signals at the start of each module mapping. The GBLF is determined by taking the first central run of each module, after the AE corrections have been applied, and finding the mean of each of the PMT's signals. The means of all the PMTs for each module are then averaged. The GBLF is then determined for each of the PMTs by:

$$G_f(i) = \frac{A}{m(i)}$$

where  $G_f(i)$  is the Gain Base Line Factor,  $A$  is the average of the PMT means, and  $m(i)$  is the mean for PMT  $i$ . This tuning factor is calculated once for each PMT and is applied to that particular PMT signal through all the raw mapping runs.

The next correction for the data is to monitor any gains in each of the PMTs during the mapping run. This correction is based on the average of each PMT for the "central" runs. The central run averages are stored along with the time (CALSEC) the central run was conducted ( Figure 4.4). The Calsec times are used to determine which of the central

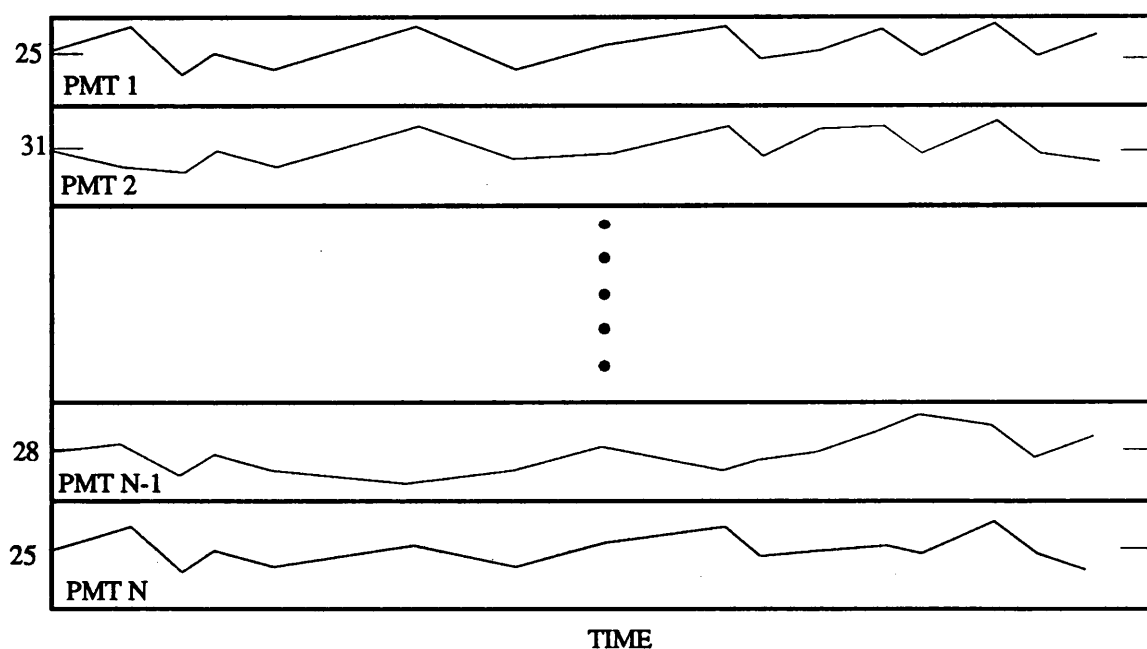


Figure 4.4 The fluctuation of each PMT is shown versus the time of the mapping process.

runs will be used in determining the Gain corrections factors. The gain factor is calculated for each PMT by interpolating between the nearest two central runs and is applied to the event signal.

The final correction to the mapping data converts the coordinates used in the mapping procedure to local module coordinates. This is done by using the coordinates of the detector center relative to the platform coordinates for that run.

## **CHAPTER 5**

### **THREE DIMENSIONAL DESCRIPTION**

The position of the collimator gives the x and y location of the center of the incident photons while the response of the PMTs is recorded. The one physical quantity that is not given, is the depth of the scintillation inside the detector. This depth information is useful in creating high resolution maps of the detectors. A technique of obtaining this information is achieved by applying Principal Component Analysis (PCA) to the set of PMT signals which span PMT space.

Principal Component Analysis uses the ratio of the PMT amplitudes to describe a new vector space which is correlated to the physical 3-D space of the detector. The following section describes how the PCA is applied and used to produce information about the event.

#### **Principal Component Analysis**

The Principal Component Analysis technique uses the best, and then successively decreasing, views of a distribution of data. The PCA works by finding a set of axes, all being mutually orthogonal, which spans the data space and best fits the distribution of the data. PCA will define the first axis such that it aligns itself with the main distribution of points. The next axis defined would be the next best fit and so forth until the dimensions of the space are spanned. The same number of axes that were in the original space or less could be used, depending on how the correlation with the data is formed. The new set of PCA axes can then be used to describe events in PMT space.

The PCA works by defining a set of axes which minimizes the distance between the distribution of data points and the new set of PCA axes. This is done by using the original distribution of data and forming a correlation matrix from it.

Let  $r_{ij}$  be the original measurements. From them a matrix  $X$  can be formed where the elements of the matrix are given by:

$$x_{ij} = \frac{r_{ij} - \bar{r}_j}{s_j \sqrt{n}}$$

where

$$\bar{r}_j = \frac{1}{n} \sum_{i=1}^n r_{ij}$$

and

$$s_j^2 = \frac{1}{n} \sum_{i=1}^n (r_{ij} - \bar{r}_j)^2$$

is the variance used to weight the elements of the matrix.

How well a new set of axes fits the distribution of data points is determined by minimizing the square of the distances between the points and the axes. This minimization is also the same as maximizing the square of the projections on to the axes. The square of the projections on to a new axis,  $u$ , for all the points is given by:

$$(Xu)'(Xu) = u'X'Xu$$

where the prime denotes the transpose. This quadratic expression can be maximized under the condition that  $u$  has a finite size. The usual condition imposed on  $u$  is:

$$u'u = 1$$

The maximization is done by setting the derivative of the Lagrangian

$$u'X'Xu - \lambda(u'u - 1)$$

equal to zero which gives:

$$2X'Xu - 2\lambda u = 0$$

or

$$X'Xu = \lambda u .$$

The quantity  $X'X$  is known as the correlation matrix  $C$  where each of the matrix elements is given by:

$$c_{jk} = \sum_{i=1}^n x_{ij} x_{ik} = \frac{1}{n} \sum_{i=1}^n \frac{(r_{ij} - \bar{r}_j)(r_{ik} - \bar{r}_k)}{s_j s_k}$$

To obtain the desired PCA axes, the correlation matrix must satisfy the equation where  $u$  is the optimum value for the solution. The desired solution to this equation is the eigenvector ( $u$ ) with associated eigenvalue ( $\lambda$ ) of the correlation matrix. Solving the equation produces the eigenvectors which are the desired PCA axes. The eigenvalue associated with each eigenvector indicates the amount of variance associated with the new axis and represents how well the axis is aligned to the distribution. The PCA axes or eigenvectors are then ranked by the eigenvalues with the largest eigenvalue corresponding to the best fit.

### COMPTEL Applications

The PCA can be used to determine information about events in PMT space [Steinle 1985] and works in the same manner as discussed above with a few variations [Morris 1986]. Each event interacting in the detector is monitored by the photomultipliers. The quantities measured are the amplitudes ( $s_i$ ) of each PMT. Each event can be represented by a vector in PMT space :

$$\vec{s} = (s_1, \dots, s_i)$$

Each event is also represented in physical space by quantities ( $x, y, z, E$ ). The  $x$  and  $y$  values represent the location of the event and the energy of the event  $E$  by the sum of the PMT signals. The quantity  $z$  is the height of the event, but is a quantity that is not measured during the mapping.

It is assumed that the interaction of the events in the detector which are along a cylinder perpendicular to the face of the detector and centered around the  $x$  and  $y$  location.

By normalizing the the amplitudes of each event, the dependance on energy is eliminated thus reducing both spaces by one dimension. This leaves only the x, y, and z quantities in physical space to describe the distribution of events.

The next step is to see how the same group of events are distributed in PMT space. This is where PCA plays a role. In forming the correlation matrix to produce the PCA axes, the amplitudes must first be normalized to eliminate any dependance of their energy fluctuation. The normalization of the amplitudes is give by:

$$n_i^k = \frac{s_i^k}{\sum_{j=1}^P s_j^k}$$

where  $s_i^k$  is the amplitude from PMT i and event k and P is the number of PMTs.

We next find the mean value for each of the PMT signals for a particular location of events within the detector. The mean values are given by:

$$\mu_i = \frac{t_b \sum_{k=1}^{n_s} n_{is}^k - t_s \sum_{k=1}^{n_b} n_{ib}^k}{t_b n_s - t_s n_b}$$

where s is the source quantity and b is the background quantity. The quantity n is the number of events in the set, and t is the live time for that set.

The PCA matrix for the event location can now be generated using the normalized signal and the means for each PMT. The PCA matrix elements are formed by comparing each normalized signal to the mean value weighted or scaled by their variance. The elements of the matrix X are given by:

$$x_i^k = \frac{n_i^k - \mu_i}{s_i}$$

where

$$s_i^2 = \frac{1}{n_s} \sum_{k=1}^{n_s} (n_i^k - \mu_i)^2$$



is the variance of the event from the mean. The correlation matrix  $C$  used to produce the new axis in PMT space is formed by taking the matrix  $X$  and multiplying it with its transpose. Each of the matrix  $C$  elements are given by:

$$c_{ij} = \frac{1}{n_s} \sum_{k=1}^{n_s} x_i^k x_j^k$$

Each mapping file is used to generate a correlation matrix unique to that particular region of the detector. Each matrix is then used to generate a set of eigenvectors and eigenvalues that correspond to that same location. These eigenvectors are correlated with the distribution of events in that region and are used to form a new PMT space called EV space. The eigenvectors that span the space are ranked starting with the largest eigenvalue and continues to the lowest eigenvalue. It cannot assumed that the eigenvalues are always easily ranked. If the distribution of events is evenly distributed in all directions, the eigenvalues will be equal in magnitude and the corresponding eigenvectors will be arbitrarily ordered.

The distribution of events in EV space can be viewed by using two dimensional scatter plots of the projection of the events on to any two of the eigenvectors. The plots can be examined to see how well the new eigenvector axes line up with the distribution of events. Some concern must be taken when generating the new EV space because both source and background events are in the source runs. The background events can play an important role in the formation of the eigenvectors by skewing the eigenvectors away from the distribution of source events.

Once the first PCA is done, the distribution of the events in EV space can be used to eliminate some of the background events. One can determine the background events by plotting the events in the 2-D scatter plots and looking at the distribution of the events. If there is little influence of the background event, the source event distribution will look like an ellipsoid and lie along the axes of the plot. If there is background influence, the plots will show an ellipsoid that is skewed from the axes and a disk of background events that

surround the ellipsoid. In order to remove background events, limits can be placed on the projections along the eigenvectors that will exclude the points that make up the disk. Using only events that fall between these eigenvector limits (EV limits), an iteration of the PCA can be done to generate a second order correlation matrix. A new set of second order eigenvectors can be produced from this matrix. With the effects of the background events minimized, these second order eigenvectors should correspond well with the distribution of source events. The same type of scatter plots can be produced using the second order eigenvectors to improve the correlation. The eigenvector limit process can be repeated until there is no change in the correlation of the eigenvectors.

Important information can be derived from looking at the largest eigenvalues and their corresponding eigenvectors. Early studies of the D2 modules show that the three largest eigenvalues and eigenvectors correspond to the three dimensions of physical space [Varendorff 1987].

The largest distribution of events in the modules is found along the z direction during the mapping process. PCA determines the direction of this distribution and aligns the highest order eigenvector along it. By using an events projection on this eigenvector ( $\lambda$ ) one can use the value to describe the depth of the interaction in the module. This  $\lambda$  value is not a linear measurement of z but can be used to describe it. A set of  $\lambda$  values can be determined for a particular x and y location, and used in place of the z parameter describing the location of an event. Regions where the ordering of the eigenvectors is well defined are known as 3-D regions. In these regions, events described by the quantities x, y and  $\lambda$ , are called 3-D events. These regions are found in the entire D2 modules, and in the regions in front of the PMTs in the D1 modules.

## CHAPTER 6

### CHI SQUARE MINIMIZATION

The algorithm presently being used for event location is a Chi Square Minimization search routine [Simpson 1987c]. Its main function is to produce an event location that corresponds to a tabled signature that best fits the input event using chi-square statistics.

The routine is given a table which contains a PMT on/off flag and a list of event coordinates with their corresponding PMT signatures. These event signatures consist of eight (D1) or seven (D2) average PMT values produced from the mapping process. The chi square algorithm is a five step process to determine the events coordinate location.

The first step is to compute the signature of the event which is a ratio of the PMT signal to the average PMT signal for that event. The signature is given by:

$$A_i = \frac{PMT_i}{\frac{1}{M} \sum_{k=1}^M PMT_k}$$

where  $A_i$  is the normalized PMT signal or pulse height,  $M$  is the number of PMTs, and  $PMT_i$  is the corresponding  $i^{\text{th}}$  PMT signal.

The second step is to determine the PMT resolution. This is first done by finding the fractional resolution  $R_i$  for each of the PMTs [Simpson 1987b]. It is used to express an expected error  $P_i$  in the amplitudes by multiplying it with the event signature:

$$P_i = R_i \times A_i$$

The third step is to limit the size of the list that needs to be searched. This is done by doing a binary search throughout the initial table using a standard deviation parameter  $Z_m$  that determines limits of map values. The limits are determined for a variable  $A_1$  by:

$$A_{\min} = A_1 - Z_m$$

$$A_{\max} = A_1 + Z_m$$

The binary search is conducted for the table values of  $A_1$  that are the last value less than  $A_{\min}$  and the first value greater than  $A_{\max}$ . The table values between these limits make up the shortened search list with the values ordered with increasing  $A_1$  values.

The next part of step 3 is to determine the contribution of the signature to the chi-square value which is given by:

$$\chi^2_n = \left[ \frac{A_1 - S_1^n}{P_1(E)'} \right]^2$$

where  $S_1^n$  is the map signature for the  $n^{\text{th}}$  point of the table. This process continues for the other signatures  $A_i$  ( $i=2, \dots, M$ ). With each repetitive cycle the table is diminished, and the total chi-square value is determined after the final cycle.

Step 4 is to look at the chi-square values of the points that are left after the selection process of step 3. This step goes through the final table to find the table value with the smallest chi-square value generated. When it is found, the coordinates associated with it are returned as the events location.

A final step may be needed if no points survive the limit selection process. Steps 1 through 4 will be repeated but with an increase of the  $Z_m$  value until a point is left at the end of the search or until  $Z_m$  reaches the value of 4.5.

There are several drawbacks concerning the the chi square algorithm. The main drawback is the large amount of computer time it takes to complete the search throughout the tabled values. Any increase in spatial resolution by using a finer grid map or adding additional table values will only add to the time required to complete a search.

A second drawback is that the event location speed is dependent on energy. As the amount of energy deposited decreases, the resolution of the module also decreases and more of the table values produce an acceptable chi square.

A third drawback is the difficulty the algorithm has in locating events which exhibit a 3-D effect. In order to locate a point from the table, with an acceptable chi square, all possible sets of amplitudes must be listed. This additional listing only adds to the time needed to complete a search of the table.

The chi square algorithm has been tested on SM-II [Simpson 1984]. The x and y error was used as the coordinates of the distribution. The accumulation of all the error for the D1 cell is shown in Figure 6.1. For SM-II, two types of resolution are used because the distributions are found to be non-Gaussian and some times non-symmetric. The first is the Full Width at Half Maximum (FWHM) and the second is the width of the error distribution that contains 67 percent of the events. The resolution determined for the SM II D1 cell was  $2.35 \text{ cm} \pm 15\%$ .

The results of this test have set the minimum requirement that any new algorithm must meet.

COMPTEL SM II D1 SPATIAL RESOLUTION

SUM OF MAPPING RUNS AT 1 MeV

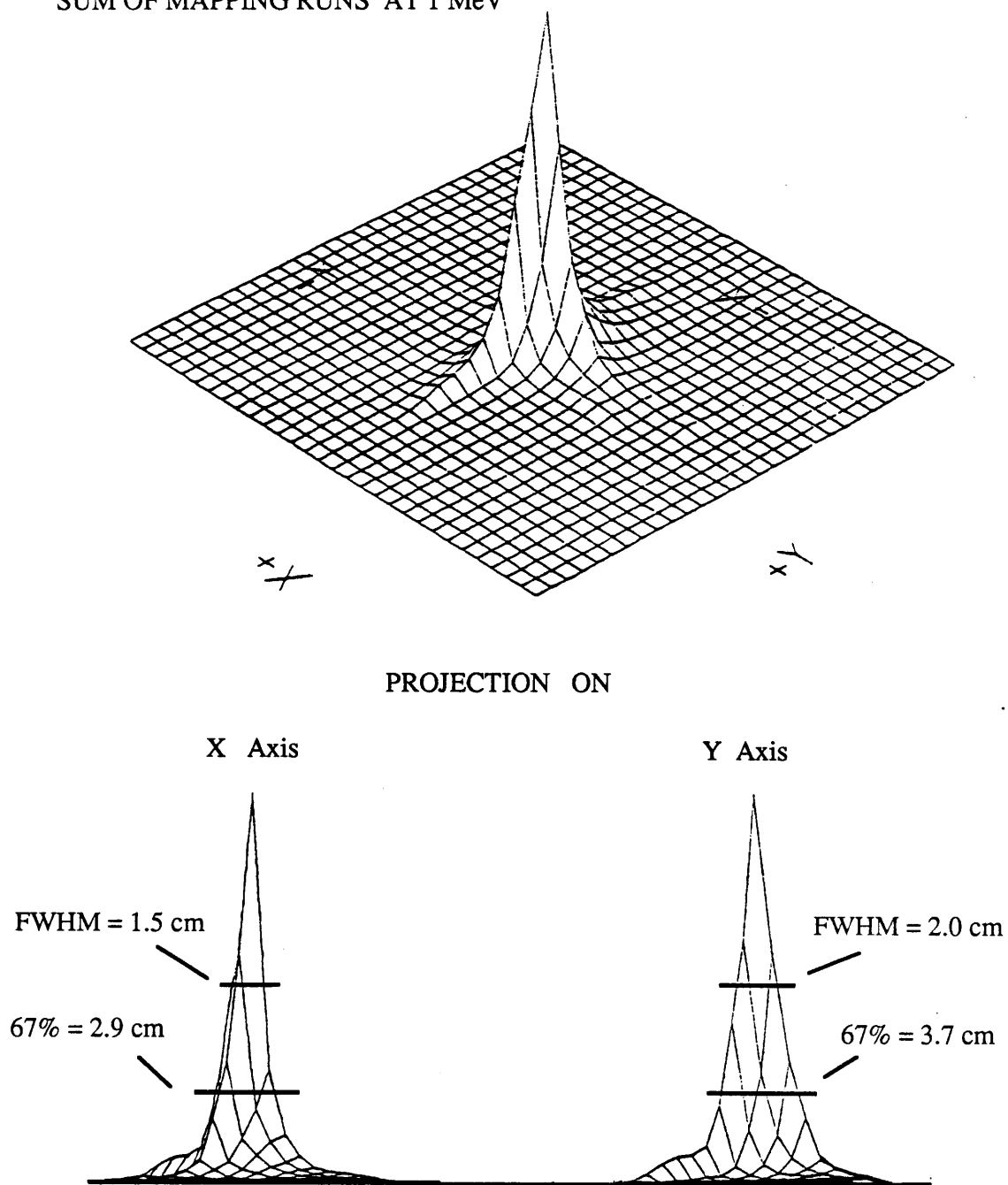


Figure 6.1

## CHAPTER 7

### NEURAL NETWORK

The neural net is a computer simulation of the human brain's connected parallel way of learning [Albus 1972]. The main structure of a neural net contains a feedback pattern that is similar to that of trial and error of the human learning function [Aleksander 1989]. The system uses a set of weights which are initially set at small random values, and begins correcting these weight values either by diminishing or increasing them depending on how well it recognizes the input values. The final weights, which the neural net converges to, make up the "memory", or knowledge of the neural net.

#### Architecture

The structure of a neural net system depends on what is required of the system. Its main architecture is determined by the information the system will learn from and the output the system will be required to supply.

Neural nets require some type of input which the neural net can learn from. The input can be in many forms such as multivariant functions [Albus 1979], words and sounds [McClelland 1988], robotic controllers [Miller 1987], and event location [Simpson 1987a]. Any type of input will work as long it contains all the information required to teach the neural net the patterns to recognize and the value that this recognition is suppose to generate. When the neural net learns to recognize these patterns it produces an output vector which should be similar to that part of the input vector with which it was taught.

For the COMPTEL neural network algorithm the input vector consists of the PMT signals and the corresponding x and y location of the source file. The system is taught to recognize the PMT signals and generate a corresponding x and y output vector.

In the main architecture of the neural net system there is not always a direct link between the input vectors and the output vectors. The requirements of the system dictate

how different weighting functions are used and the number of processes which exist between the input and output values.

For the event location neural network there are three weighting parameters which are used to control the connections between the input and output of the system. They are Beta, PMT scaling (SCP), and Generalization parameters.

The Generalization parameter is used to define the number of cells in the neural net memory which will be used in determining the response vector. The selection of the memory cell to be used is assigned by an indexing system which is a combination of the input vector value and the Generalization parameter.

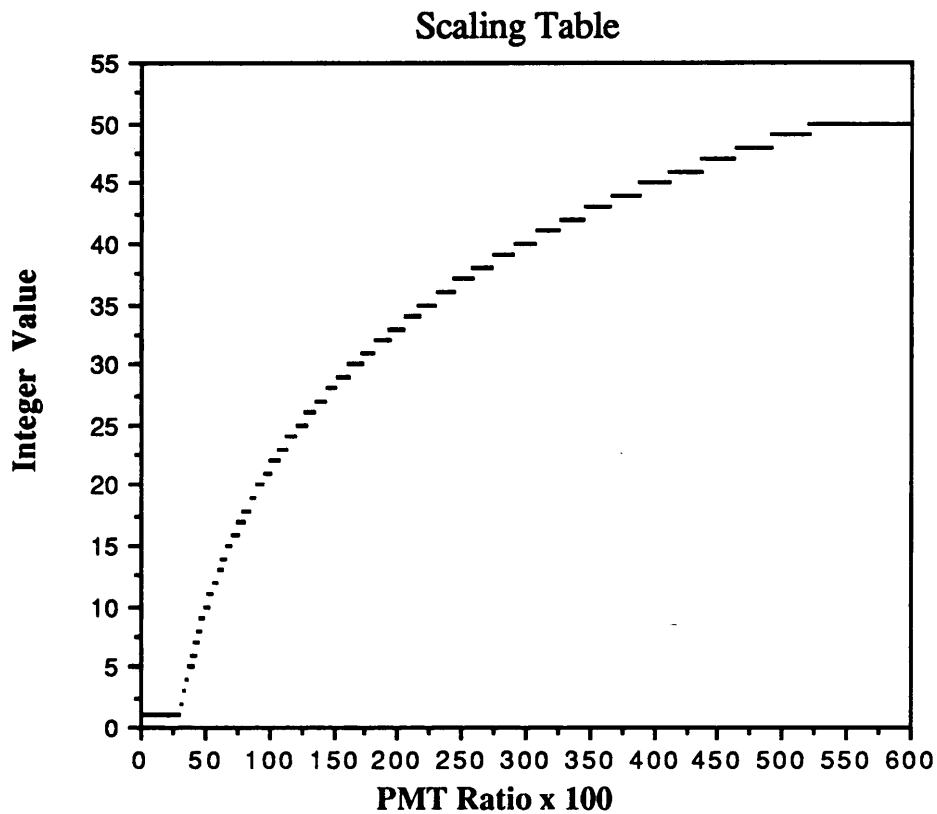


Figure 7.1 The logarithmic PMT Scaling Table. The PMT signals are converted to integer values by use of the scaling table which is controlled by the SCP parameter

A scaling process is introduced to handle the larger range of PMT signals and to quantify them into integer values which are a requirement of the neural net. This scaling



process is controlled by the PMT scaling parameter (SCP). It is used to determine the assignment of logarithmic values in an array. The PMT signals are then used to determine which array value will be used to represent it in the indexing of the neural memory. Figure 7.1 shows a typical range of the logarithmic array used in the scaling of PMT signals.

The Beta parameter is the controller of the learning process of the neural net algorithm. It is a damping factor used to determine how much correction is applied to the memory cells used in determining the output vectors. Figure 7.2 shows the structure of the neural network and the interface of the controlling parameters.

### **Learning**

The learning process of the neural net consists of a set of examples in the form of input vectors from all possible locations. Each set of input vectors is consecutively sent to the neural nets so as not to weight the memory to one particular response. The input vectors that are used consist of the PMT signals for an event and the corresponding location of the collimator. The location, in this case an x and y coordinate, is the targeted response that the neural net should produce when presented with the other part of the input vector.

The first set of output vectors will be randomly distributed because the initial weights start off small. In this case the weights are zero. The memory of the neural network is taught through a technique of back propagation [Jones 1987]. This technique is the adjustment of the memory using the delta rule after the response of an event is given by the neural net. The delta rule is part of the program that is designed to calculate an error between the targeted value and the one produced by the neural network. The error is distributed proportionally among the weights that were used to produce the output vector. The delta rule is expressed by:

$$\Delta = \frac{\beta (R_T - R_S)}{C_n}$$

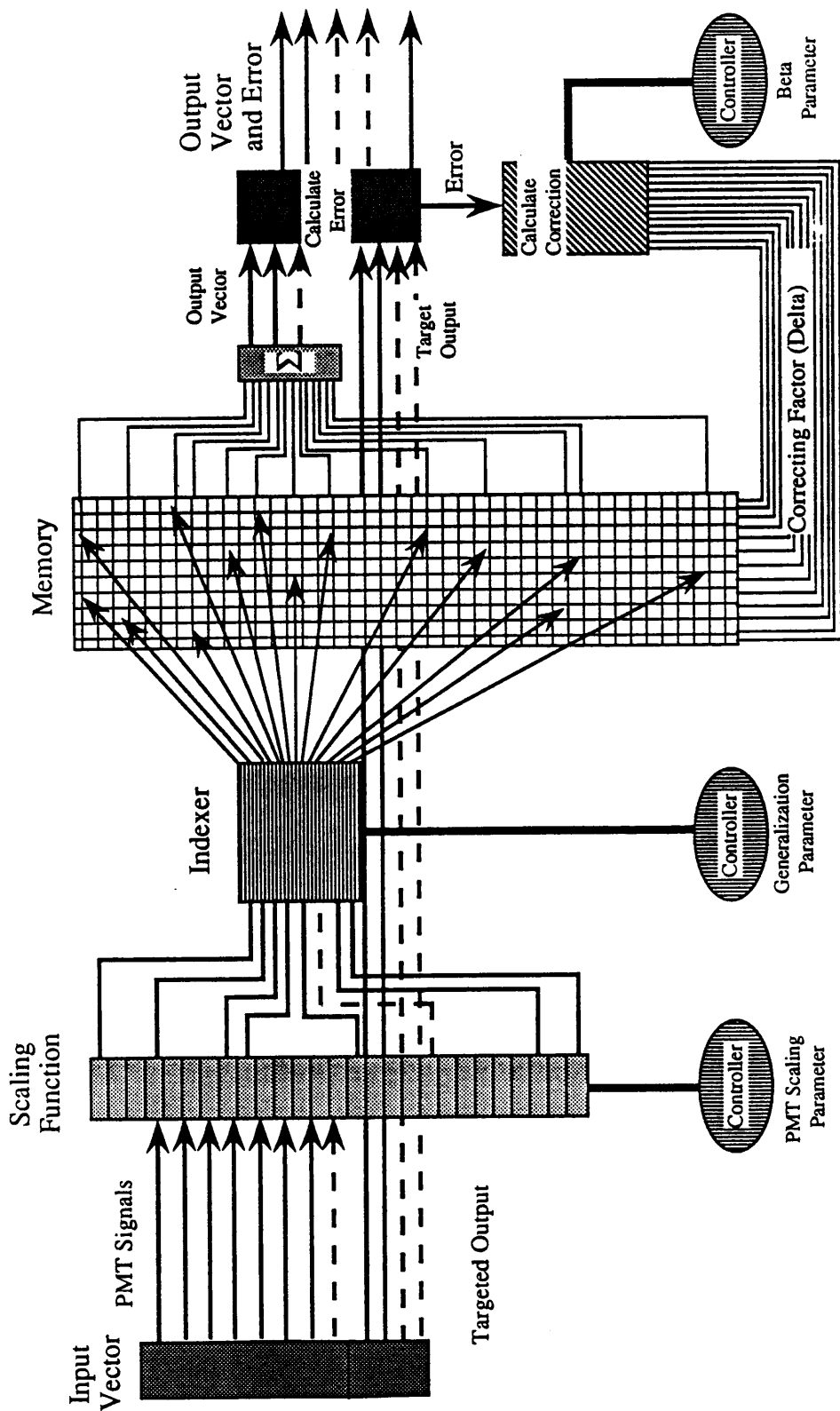


Figure 7.2

where  $\Delta$  is the change added to the memory,  $\beta$  is the damping or weighting value of the learning response,  $R_T$  is the Targeted response and  $R_S$  is the output response of the neural net system. Figure 7.2 shows the structure of the neural net that is used for the event location in the detector.

Another set of input examples is presented to the neural net where the weights are again adjusted using the back propagation routine. This process continues until the weights converge to values which allow the neural net to recognize most of the examples in the learning set. If the weights do not converge to give the desired response the parameters are changed, and the neural net is retrained with the new parameters. This process continues until the weights give a reasonable response.

### Testing

When the neural net has had ample events to learn on it is tested to find how well the memory can reproduce the needed output. During the learning cycle the back propagation portion of the algorithm is turned on and the neural net will learn by adjusting the weights. The testing is conducted simply by turning the back propagation off and allowing the neural network to locate or remember events without any adjustments to the memory. A fully taught neural net can be tested using the same types of events or even the actual events it learned with. The reliability of the neural net is then be accumulated statistically by comparing the targeted vector to the response vector. The error is given by the square root of the quadratic sum of the differences in the two vectors:

$$ERR = \sqrt{(R_{xT} - R_{xS})^2 + (R_{yT} - R_{yS})^2}$$

where  $R_{xT}$  is the x Targeted response and  $R_{xS}$  is the x output response from the neural network.

## **CHAPTER 8**

### **TEST RESULTS**

The testing of the neural net algorithm consists of three parts. The first part is determination of the parameters that will maximize the learning capabilities of the neural net algorithm. In this phase of the testing Beta, SCP, and the Generalization parameters are changed and evaluated for different learning cycles. The second phase teaches the neural net using a set of mapping runs that cover one quarter area of a module. In this phase the spatial and energy resolution of the neural net algorithm is evaluated and its event location speed is determined. The third phase consists of learning using mapping runs from an entire module. The spatial resolution of the algorithm is determined for individual points and the entire module. The final part of this phase uses a flood test that is conducted using a set of background files that were taken over the entire area of the module.

#### **Parameter Test**

The first test was the evaluation of the controlling parameters. This was done by allowing the neural net to learn with a set number of events from source files, and then testing its event location capabilities for a number of test events from those same files.

Part of the neural network is set at the end of a learning cycle to monitor the statistics of the learning progress. This is done by locating a preset number of events and monitoring the error of the neural net's output vector compared to the targeted input vector. The error is compiled, and at the end of this "remember cycle" a Root Mean Square (RMS) error is produced. The number of learn and remember cycles continues until all the events in each of the source files is nearly exhausted. After the first full cycle the elimination of background events is performed by using the neural memory to locate the input event prior to the learning process. If the error of the event is more than 2.5 times the RMS value, the event is rejected and not used for learning. The determining factor of how well the neural

net learned to locate events is the RMS or resolution. This is represented by a learning curve where the resolution is plotted versus the test cycle. After the last cycle is completed the timing and memory statistics are displayed. These statistics are the amount of CPU time it takes the neural net to remember all of the test events and the amount of memory needed to store the indexing cells used to produce the output response.

The Generalization parameter is the number of cells that are used to determine the response vector of the neural net. The initial runs start with the generalization number between the range of 10 and 100. Figure.8.1 shows learning curves of different variations in the Generalization parameter with the other two weighting functions set.

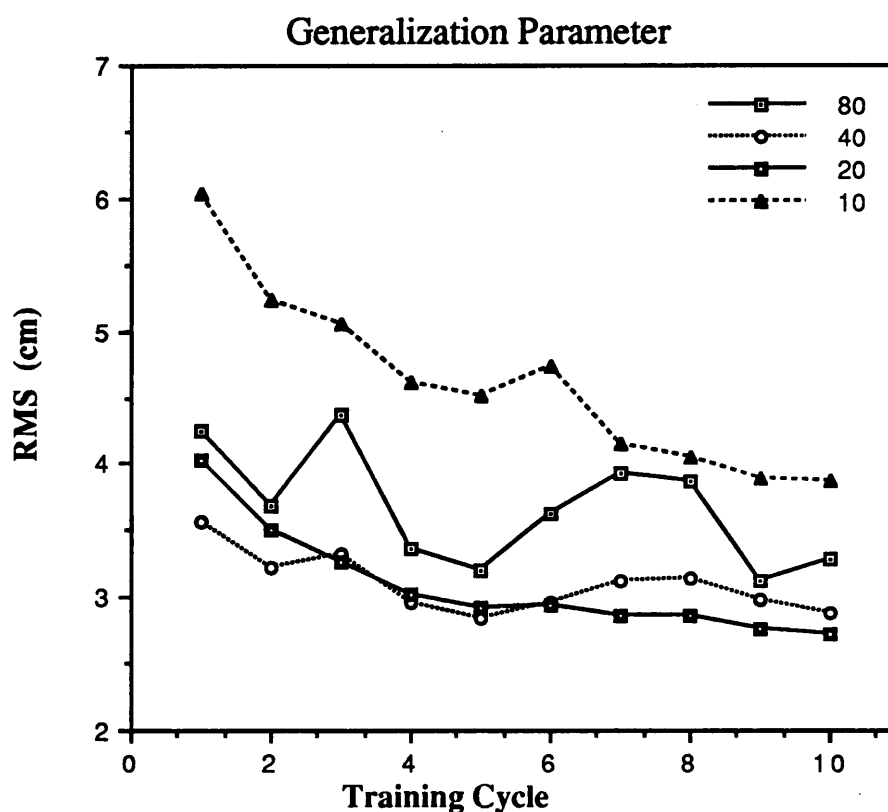


Figure 8.1 The learning efficiency of the neural network is demonstrated in the learning curves. Here the resolution averaged over all the mapping runs is plotted against the training cycle number. Repetitive learning shows how the weights will usually converge to produce a value close to the desired output.

The rate of event location is relatively important and has to be considered along with the resolution. Early testing indicate the size of the generalization parameter is related directly to the time of event location. Any increase in the Generalization parameter corresponds to an increase in the time required to locate events. It is the generalization parameter which dictates the rate of the event location, while there is little influence from Beta and SCP parameters. Figure 8.2 shows this correlation between the event location speed and the resolution for different values of the generalization parameters. One of the interesting results is that with the correct choice of Beta and PMT scaling parameters, any Generalization parameters could achieve the same final resolution.

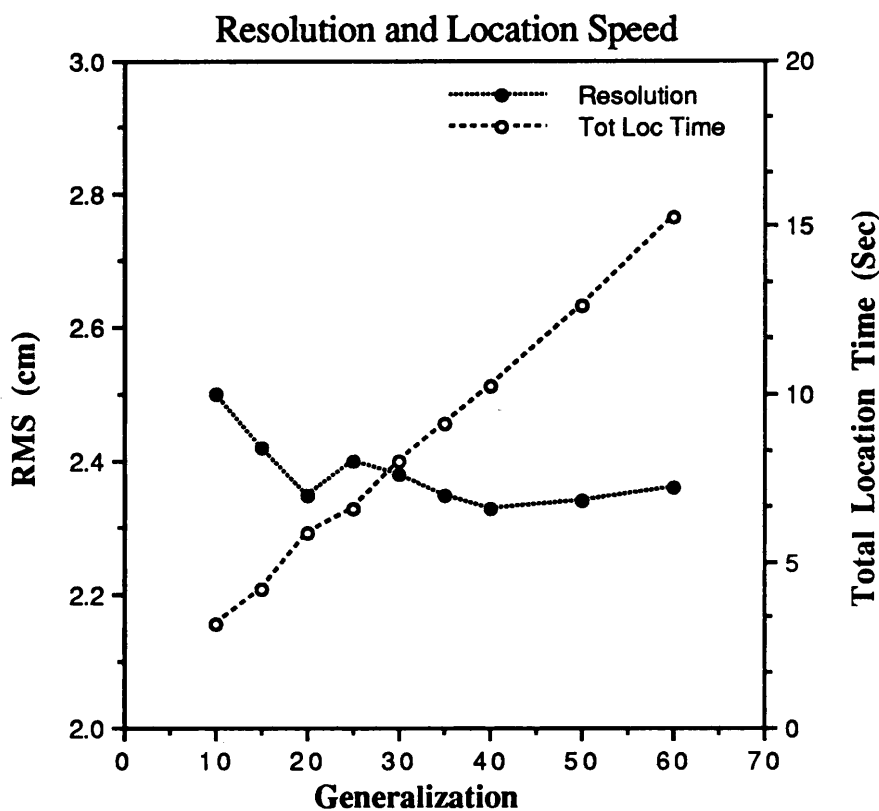


Figure 8.2 The correlation between event location time, resolution and the Generalization parameter. The Beta and SCP parameters were not the same for each of the Generalization values, but were chosen to produce the best possible resolution.

Beta is the damping factor of the delta rule which determines how much the neural net will learn from each of the test events. Smaller values of Beta allow minimal adjustments, while large values allow greater changes in each weight that is used in forming the output response. If large changes are allowed it will remove any information learned from previous events. If this happens, the weights are never allowed to converge and produce consistent results. Figure 8.3 shows that large values of Beta produce large fluctuations in the learning capabilities of the neural net.

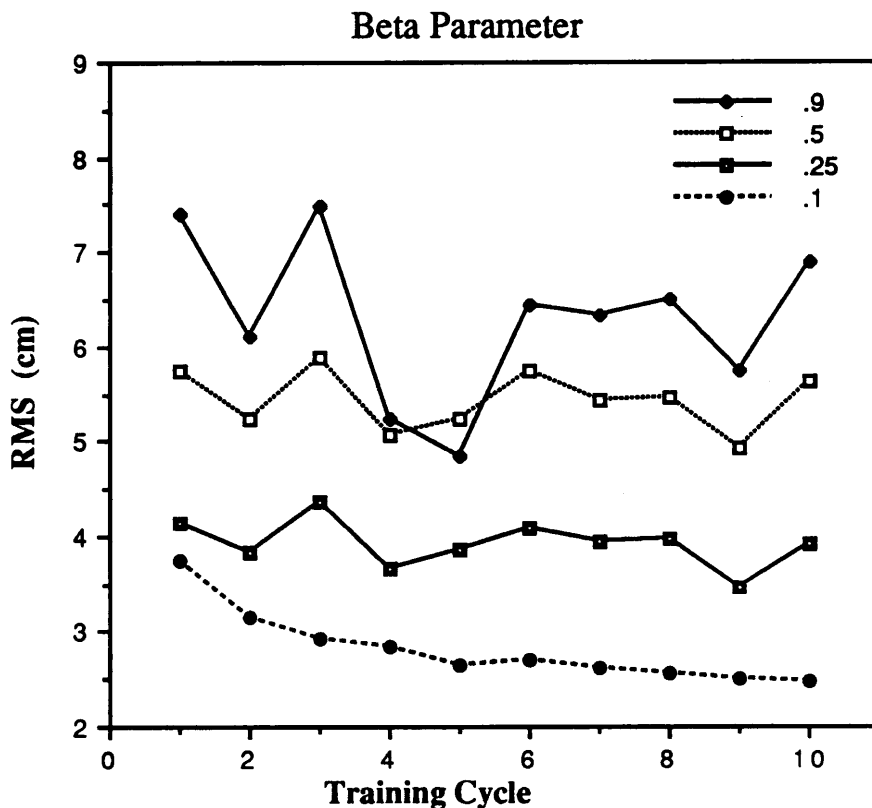


Figure 8.3 The influence of the Beta parameter. Larger values of Beta allow the memory to overlearn from new events and in the process forgetting about past events.

The third adjustable parameter is the SCP (PMT scaling parameter). Figure 8.4 shows how the adjustments on the SCP change the learning capabilities of the neural net.

This parameter sets the logarithmic range of integers that will represent the signals in the operations of the neural network. Small SCP values produce a large range with a finer division in the array of integer values that can be assigned for the PMT signals.

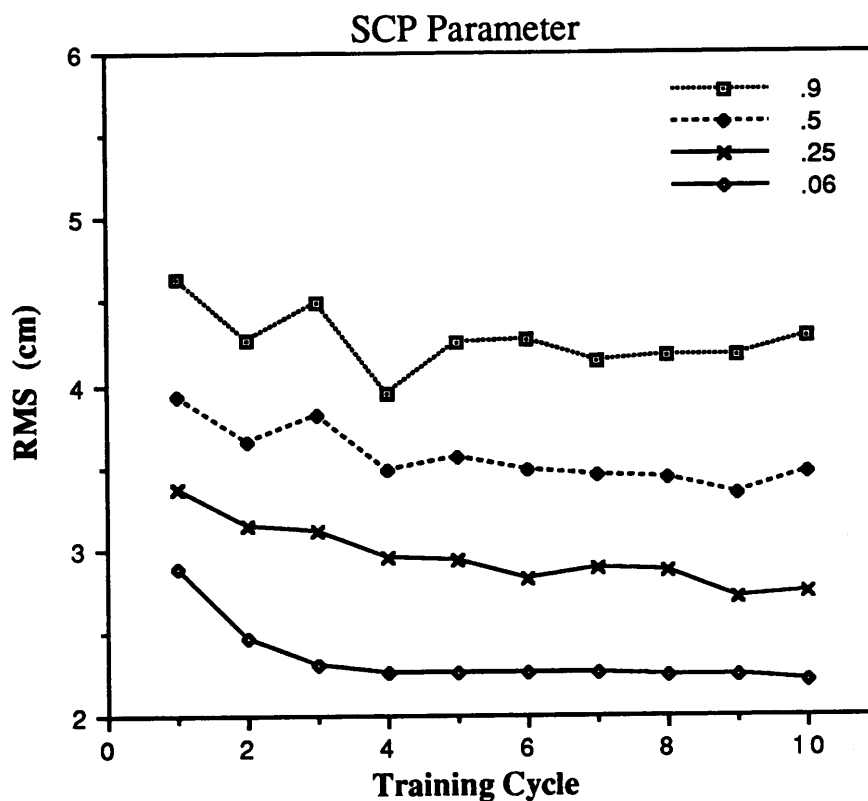


Figure 8.4 The effects of the SCP (PMT scaling parameter) on the learning capabilities of the neural network is shown. Large SCP produce a small and limited range of integer values that will be assigned to the input vector for neural learning.

The final parameters that were chosen for the remaining neural net test are:

Generalization = 20

Beta = .05

PMT scaling = .06



These values produced the best resolution for the region tested while maintaining a fast event location speeds.

### Quarter Module Test

After the variable parameters were determined, a larger scale test was conducted over one quarter module. The test was designed to determine the characteristics of the neural net learning for a large selection of events with different x and y locations and thresholds.

The area tested contained 235 mapping runs consisting of all three threshold runs. The limiting factor in this larger scale test involved the amount of disk storage space available to hold all the event information for each of these runs. A temporary solution to this problem was to store only 1000 events from each of the mapping runs on the computer disk. This allowed all the files to be present for learning and allowed a large enough sampling for the neural net to properly learn and test on.

An energy window is placed on the events in order that most of the events are near the 1 MeV energy range which corresponded to the D1 Sum value of 215. The lower and upper limits of the D1-Sum window were set at 195 and 230. Figure 8.5 shows the learning curve of the neural net for the quarter module test.

After the neural network had learned over one quarter of the module, the back propagation portion of the algorithm was turned off and neural net was allowed to locate the events using the same set of files that it had learned with. The RMS resolution, over the quarter module, was 2.21 cm. RMS statistics were accumulated for each of the mapping points and used to generate a contour image of the resolution as a function of position. Figure 8.6 shows the contour of the of the resolution for the quarter module area.

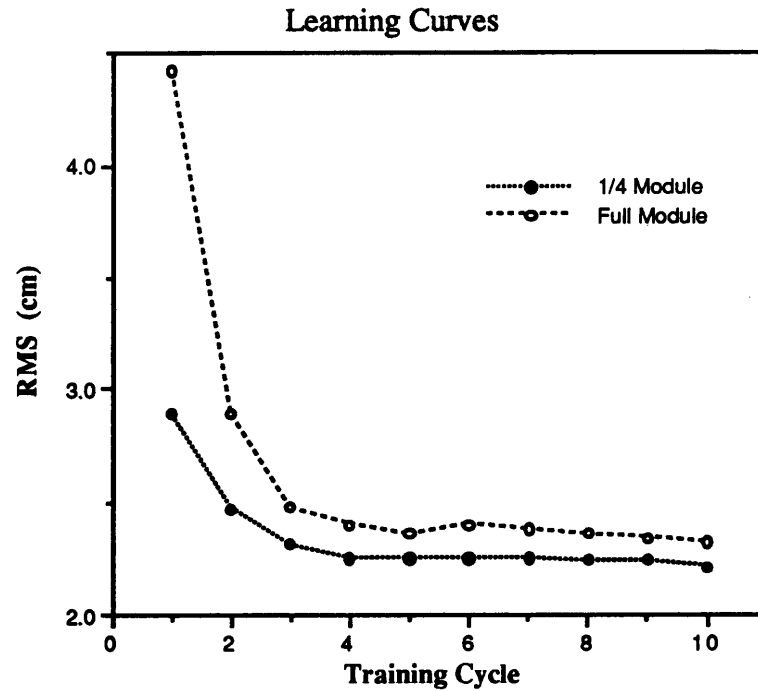
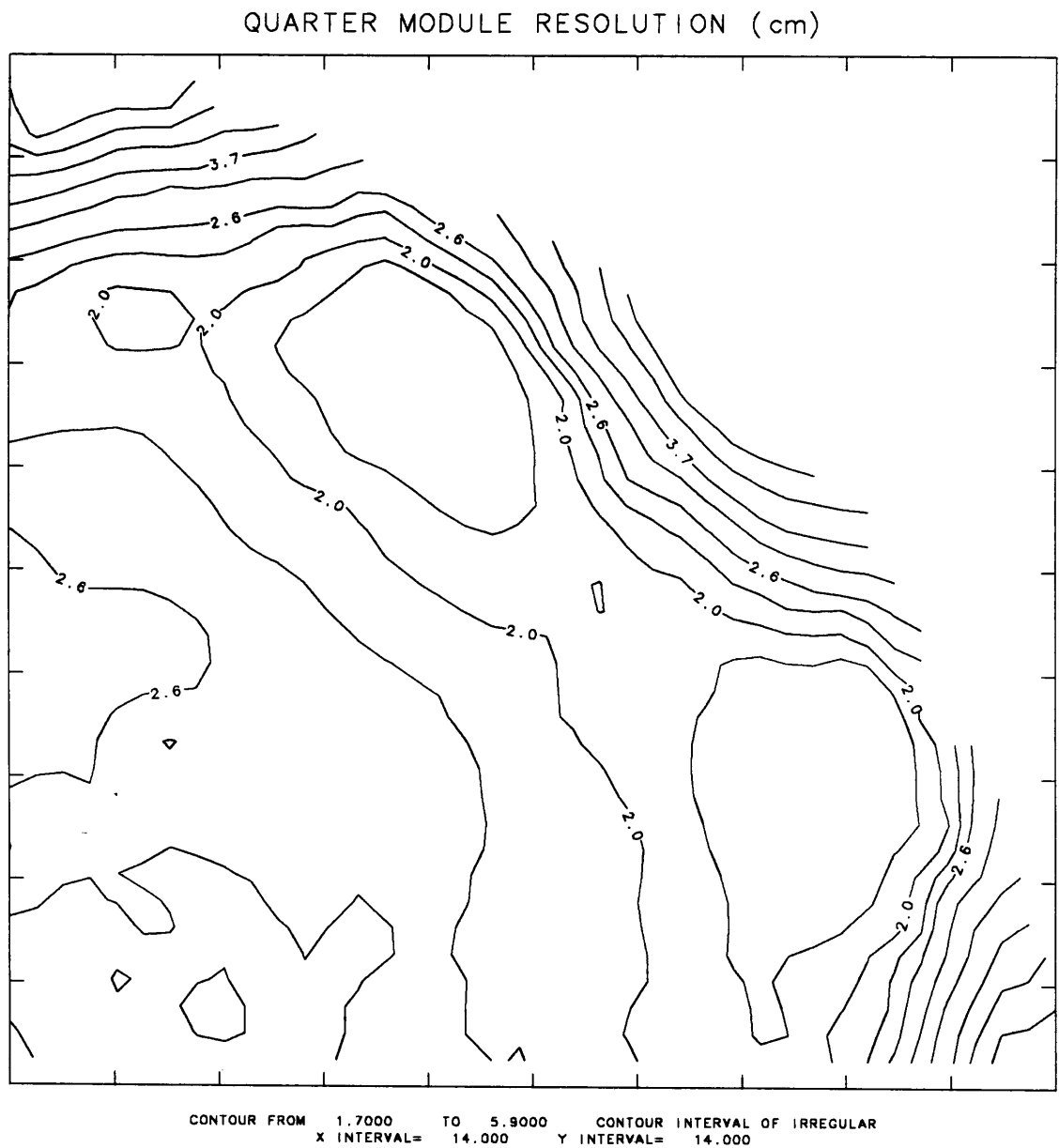


Figure 8.5 The Learning Curve for the one quarter and full module tests.

The next step in the quarter module test was to see how well it would locate events at different energies. This was done by selecting the open window runs which contain events over the entire range of detectable energies of the D1 system and using events of certain energies by setting the threshold window limits. Seven sets of tests were conducted at different energy windows with the resolution and event location speed monitored. Figure 8.7 shows the resolution for each of the D1-Sum windows. The figure shows the resolution is a function of the inverse of the square root of the energy. This test shows how the neural net can

Figure 8.6 Resolution Contour as a function of position. The contour is for the region of one quarter module containing source files with only positive x and y values.



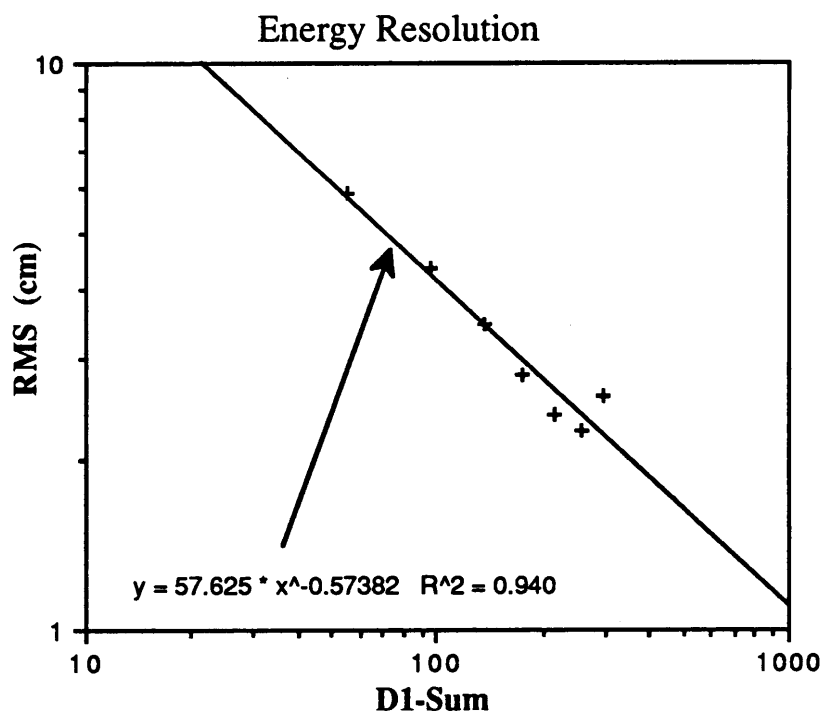


Figure 8.7 Resolution as a function of D1- Sum (Energy).

locate events at both lower and higher energy ranges while using a memory that was created using events in the 1 MeV range.

The final test for the neural net over the quarter module was to see how fast the neural net could locate events. This location rate however is computer dependent. The computer used at UNH to test both the neural network and chi square algorithms is a Prime 6550 (Panther). The first test of speed was conducted at the 1 MeV energy range where it located events at the rate of 1,282 events per second of CPU time. The next step was to test using the same seven energy windows used in the resolution test. Figure 8.8 shows the rates at which the neural net located and how it is energy independent.

In comparison, the chi-squared algorithm works at 92 events per second CPU time in the 1MeV energy range. Figure 8.8 also shows the rate of event location for the neural network and chi square algorithms for the corresponding energy window.

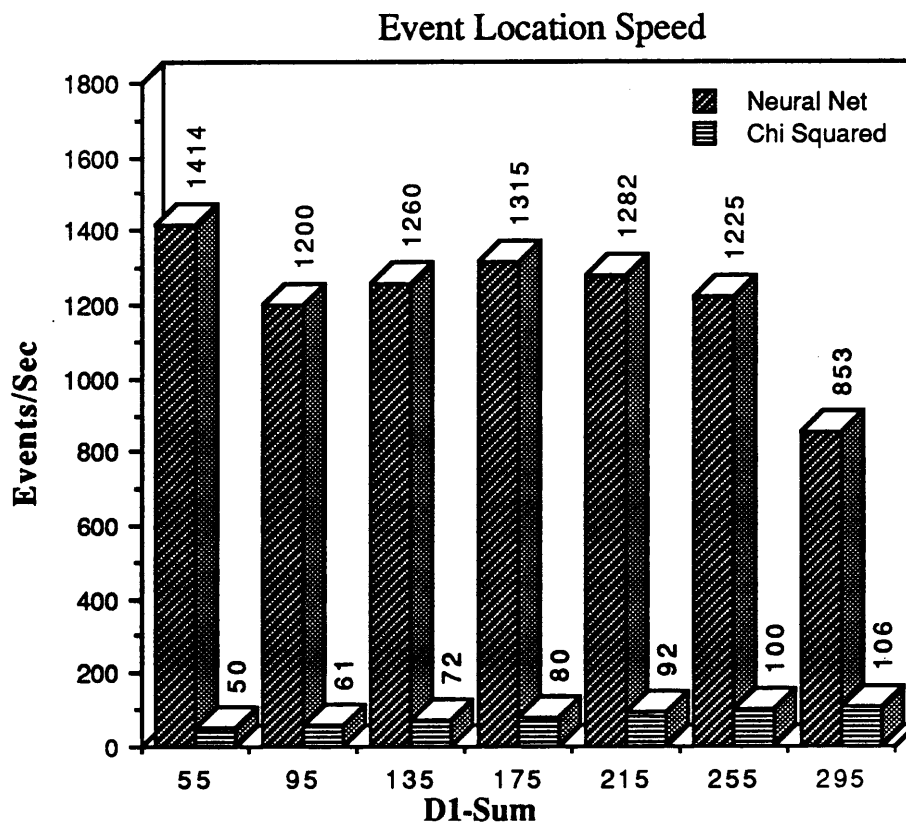


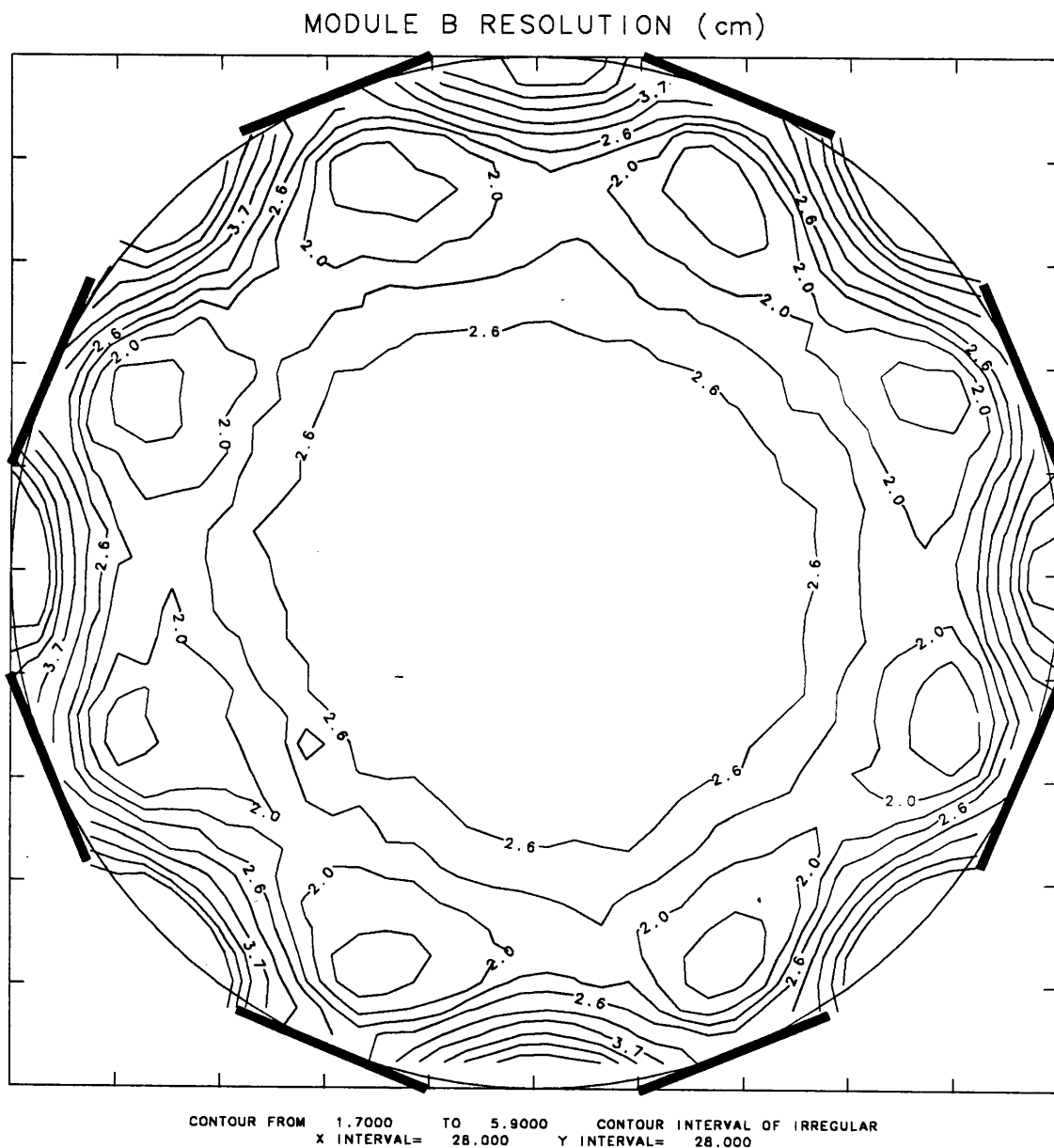
Figure 8.8 Event location Speed of the Neural Network and the Chi Squared Algorithms.

### Full Module Test

The largest scale test for the neural net algorithm was in learning the entire set of module mapping runs. The problem with limited disk storage was solved during the quarter module testing so that all the mapping runs, consisting of 920 files, could be stored on the disk with all events from each run included. The same set of parameters from the quarter module test were used in the generation of the neural nets memory for the entire module. Figure 8.5 shows the learning curve of the neural net for the full module test.

The RMS resolution of the neural net over the entire module was 2.31 cm which is very close to value of the quarter module test of 2.21 cm. The same set of statistics that were monitored in the quarter module test are used to produce a contour resolution as a function of position for the entire module. Figure 8.9 shows the resolution is a function of location for the module.

Figure 8.9 Resolution Contour as a function of position. The contour is for an entire quarter module. The location of the PMTs is represented by the dark lines about the edge of the module. The contours shown have values of 1.7, 2.0, 2.3, 2.6, 3.1, 3.7, 4.5, 5.2, and 5.9 cm.



The central region of the module is found to be uniform in resolution. This factor is not surprising because there is little variation in signals from events in this area therefore the resolution is expected to be similar. The areas of best resolution are found in front of the PMTs showing that the neural net can learn from events that show a 3-D effect. The areas that show the worst resolution are located between the PMTs. The percentage of the module area containing a maximum resolution is shown in Figure 8.10.

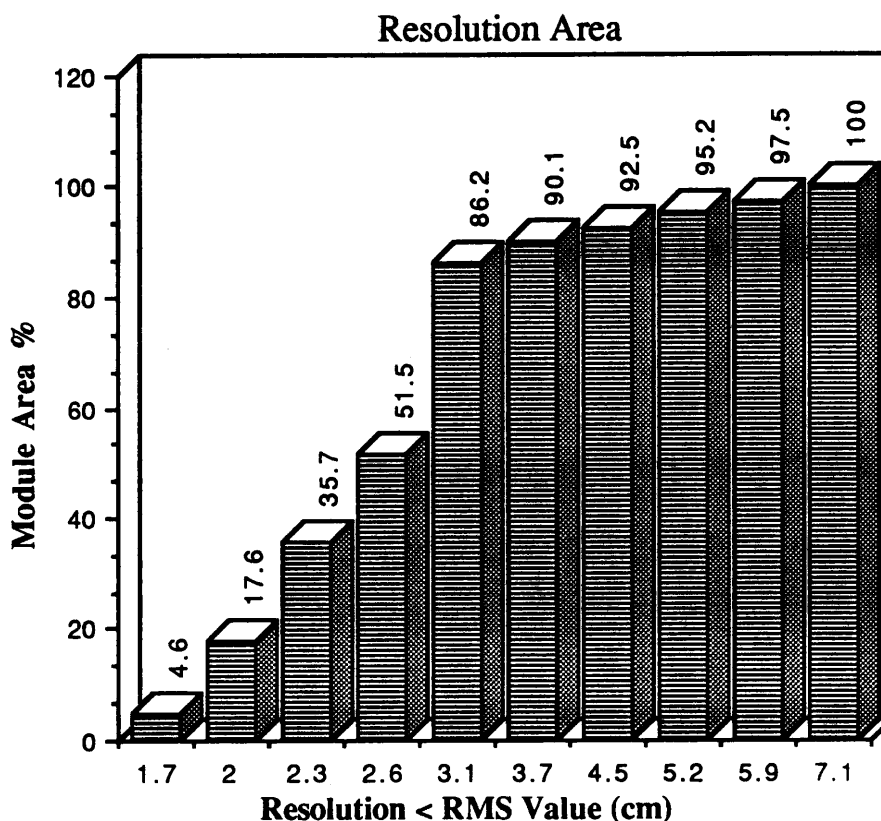
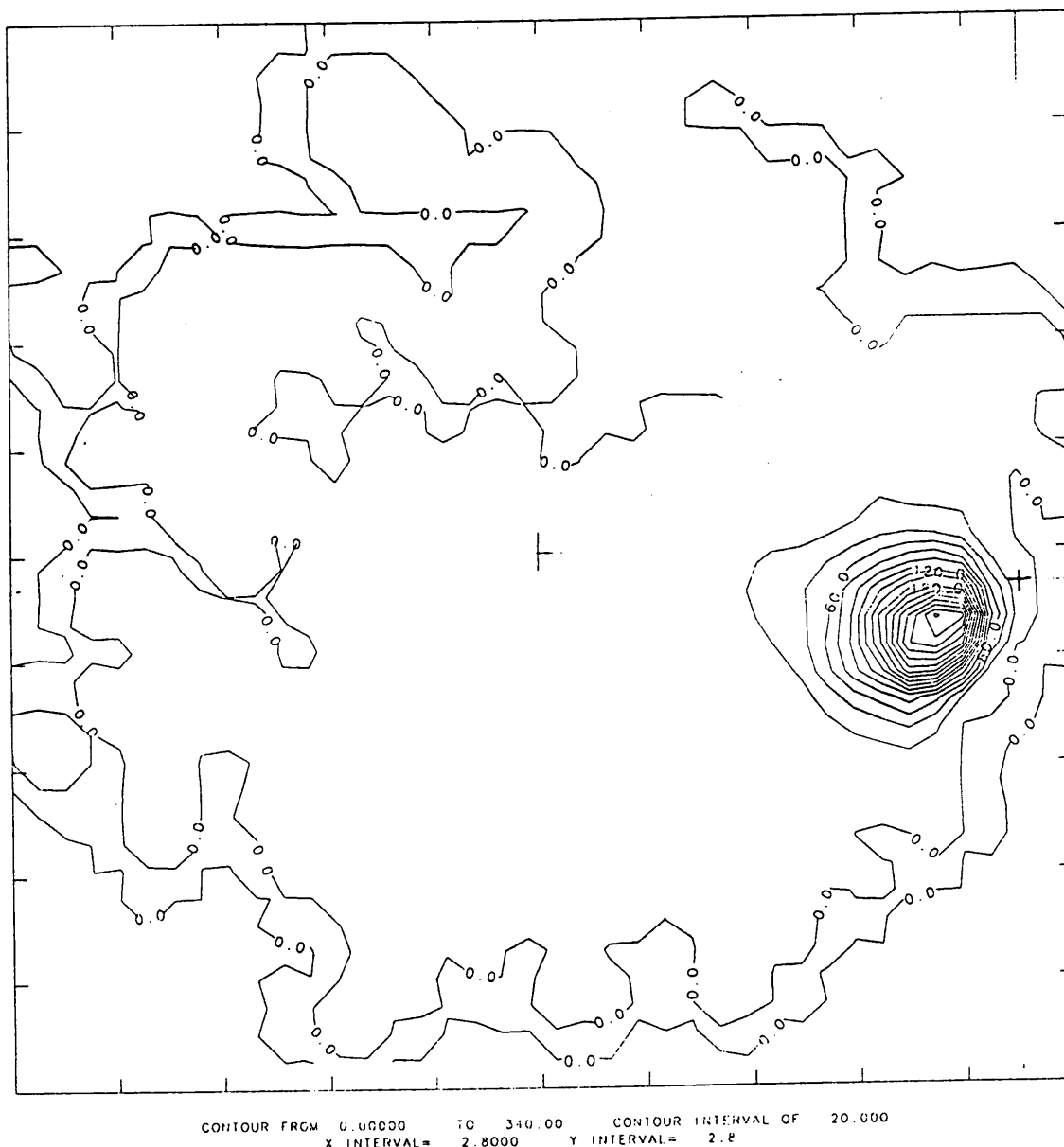


Figure 8.10 The area of a module with resolution less than the RMS value.

A series of tests were conducted to find out where the neural network was locating the event from files in these areas. Several files were used with the neural net in the remember mode, and a location array was used to monitor where the neural network located events from these files. The location array was used to produce a series of contour plots of where the events were being located. The contour of the event location from a

source file located between the PMTs and along the edge of the module is shown in Figure 8.11. The reason for the low resolution in the areas between the PMTs is that the neural net algorithm is locating events toward the center of the module and not in the outer regions.

Figure 8.11 Contour of the event location from a source files located along the edge of the module and between the PMTs. The + on the plot indicates the location of the collimated beam.





### **Background Flood Test**

The last test for the neural net algorithm was a flood test of background events. A flood test is conducted by using only background files that are evenly distributed over the entire module. What is expected from these files is an even distribution of events across the area of the module. Any discrepancies in the event location should be revealed through the location of this even distribution of an expected 98 events per square centimeter. Figure 8.12 shows the contours of the event location for the background flood test.

One characteristic revealed with the flood test is its event location distribution between the PMTs. Figure 8.12 shows that in the event distribution there are eight peaks located in front of the PMTs while no events are being located between the PMTs. An event location test was conducted with the neural network attempting to duplicate these peaks and hollows. The test consisted of determining where the neural net locates the events from source files that have coordinates between the PMTs. Figure 8.13 shows how the distribution of the events were located in the region in front of the PMTs or further in to the central part of the module instead of at the module's edge. The contour is similar to the one produced from the background flood test. This similarity of contours indicates that the peaks found in the flood test are formed from the events that should be located in the hollow areas.

Figure 8.12 Contour of the event location for the background flood test. The average value expected is 98 events per square centimeter.

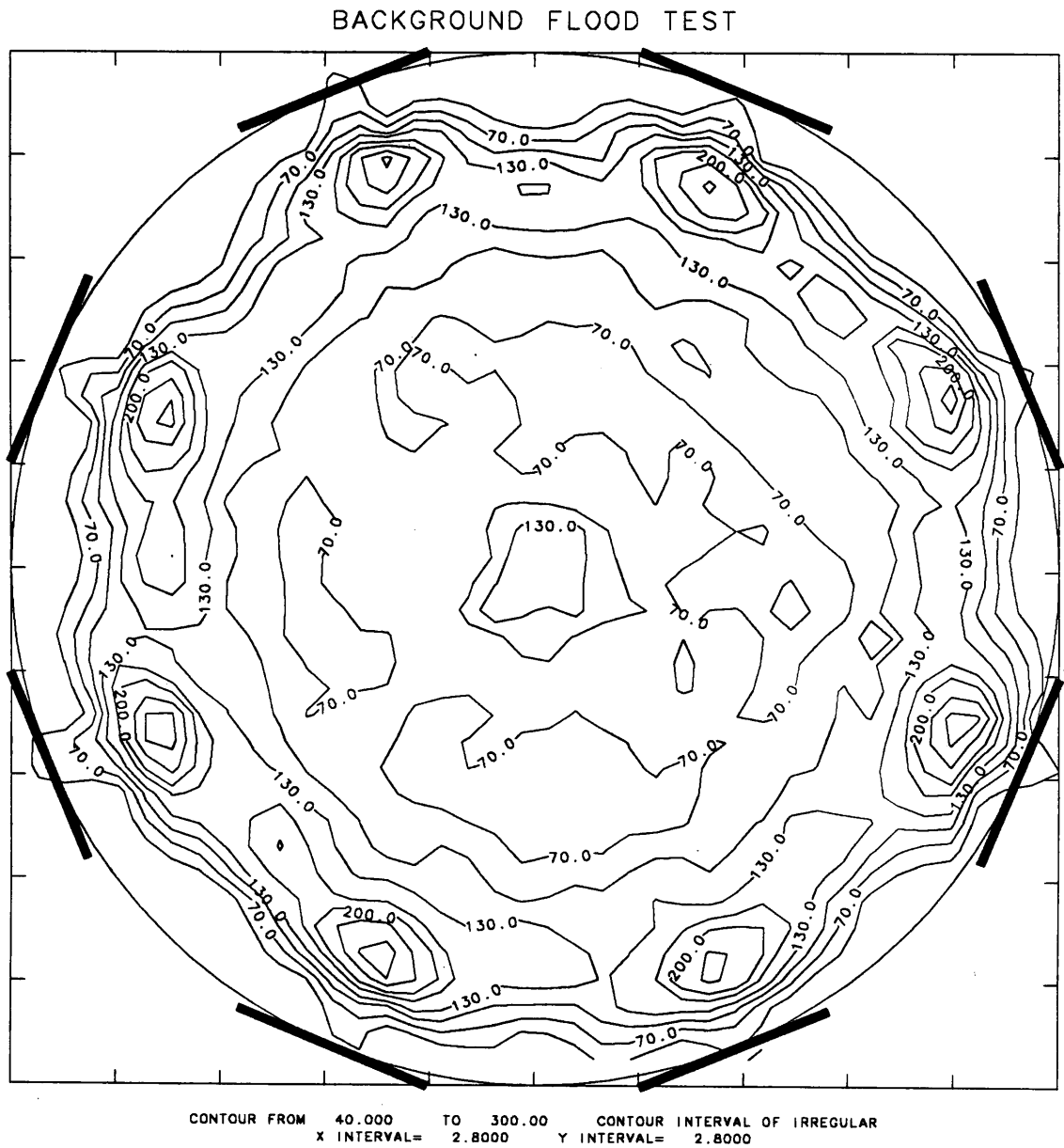
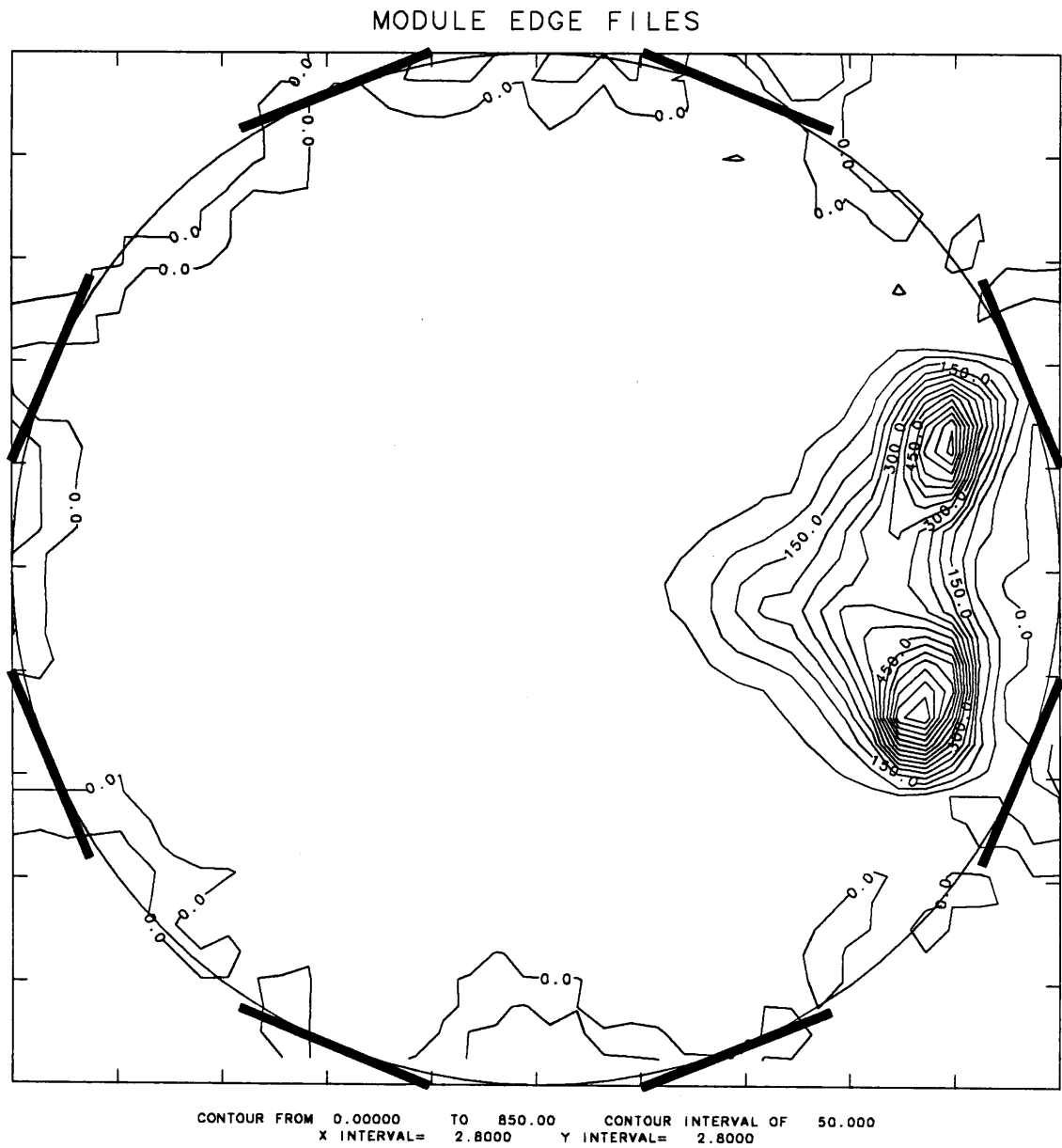


Figure 8.13 Contour of the combined event location from four source files located along the edge of the module and between the PMTs.



## **CHAPTER 9**

### **DISCUSSION**

A new Anger Camera algorithm is being developed at the University of New Hampshire. This new algorithm uses a neural network to spatially locate events in the detectors of the Compton Telescope (COMPTEL) on board NASA's Gamma Ray Observatory (GRO).

A set of module mappings is performed which relates the spatial location of an event (physical space) to the response of the detectors (PMT space). This set of mapping data is corrected to insure the proper production of a map, and is then used to teach and test the neural network capabilities.

The evaluation of the neural network's learning capabilities for an entire module was conducted in a series of tests. The first test determined the three variable parameters which govern the neural network's learning skills and its speed of event location. The second test used these parameters and the mapping runs from one quarter module to teach the neural network. The final test used the same parameters and the mapping runs from an entire module to determine the overall cell resolution capabilities of the neural network. The following is a summary of the results.

#### **Chosen Parameters**

The neural network uses three variable parameters to adjust its learning capabilities. The Generalization parameter determines the number of cells from the neural memory to be used in forming the response of the network. This parameter was found to be directly related to the speed of event location. The SCP (PMT scaling) parameter is used to form a logarithmic scale that is used to convert the PMT signals in to integer values which are used by the neural network. The SCP value determines the size and number of divisions in this

scale. The Beta parameter is used to determine how the memory is adjusted from the learning experience of an event. Tests were conducted to determine the best possible combination of these three parameters for producing high resolution and quick event location speed. The values of these parameters, which satisfied these requirements, were determined to be Gen. = 20, SCP = 0.06 and Beta = 0.05.

### **Quarter Module Test**

The second step in the evaluation of the neural network was done by using the mapping runs from one quarter of a module and the three parameters values determined earlier. This test determines whether the neural network can perform as well as the chi square algorithm previously used for event location.

The neural network was tested using 241 source files. An energy window was used which allowed only events with energies in the 1 MeV range to be used in the teaching process. The determination of learning accuracy is done by using the Root Mean Square of the targeted x and y output and the x and y values given by the neural network. The average quarter cell resolution for the 241 runs is 2.21 cm.

After the neural network had learned in the 1 MeV range, it was tested at lower and higher energies. The testing was done using a set of open window runs which contained events of all energies. The energy window was adjusted to allow only selected energy events to be used in the testing. Statistics showed the resolution was a function of the inverse square root of the energy.

Using the same set of open window runs, the event location speed of the neural network was tested. The same energy windows used in the energy resolution were again placed on the neural network as the algorithm located events. Results indicate that the neural network located events 15 times faster than the chi square algorithm. It also showed that the neural network event location speed is energy independent. A major problem of the chi square algorithm is that the event location speed is energy dependent and thus slows down at lower energies.

### **Full Module Test**

After the evaluation of the neural network's performance on the one quarter module, final testing was done to determine how it would perform when taught for an entire module. This test used 920 mapping files which cover an area of a full module. The same 1 MeV energy window was used to produce events to teach the neural network. The average resolution found for the module is 2.31 cm, which is a slight improvement over the SM II D1 module resolution of  $2.35 \text{ cm} \pm 15\%$  produced using the chi square algorithm. The regions with the highest resolution are located in front of the PMTs which are the 3-D regions of a D1 module. This shows the capabilities of the neural network to learn from and locate events which exhibit 3-D effect without being taught the  $\lambda$  values. Regions between the PMTs are found to have the worst resolution. To find the reason for this low resolution event location tests were done using source files in these areas. The tests indicate the events from these files are being located in front of the PMTs or towards the center of the cells instead of along the edge of the module.

This final test of the neural network also consisted of a background flood test designed to produce an even distribution of events in the module. The locations given by the neural net were used to produce a contour plot of the distribution. This distribution would indicate learning patterns of the neural network. Results of the contours show the neural network locating events in the regions in front of the PMTs that should be between them. This same pattern was seen earlier from the low resolution tests. The event peaks in front of the PMTs could be reproduced by locating the events from source files located between the PMTs and along the edge of the module. Comparison of a similar flood test, using the chi square algorithm, shows a similar contour pattern for the module.

### **Maximum Resolution**

The maximum resolution that the neural network can achieve is dependent on some of the physical constants in the mapping process. A major limitation is the collimated beam designed to have a 1 cm diameter at the bottom of the module. Scattered electrons are

produced along this beam which will begin to travel in different directions depending on the energy deposited. This scatter direction can contribute to determining the resolution, because the electrons can distribute energy outside the beam volume. The electrons with the largest range are produced in the energy range of 1 MeV. These electrons can be expected to travel, at most, 0.5 cm through the NE213A material. At this energy they will start to travel in the direction of the collimated beam before scattering through the material. This will contribute little in determining the volume of scintillation. The major influence of the limiting resolution is thus the collimated beam size which will not allow an approximate RMS resolution better than 0.5 cm.

If an event happens close to a PMT, allowing it to receive a large majority of the light while the other PMTs do not receive enough to help determine the location, there is a limiting effect for the expected resolution. The limiting factor is no longer the beam size but the physical size of the PMT. The resolution becomes a function of physical size and determines how precisely the event can be located. For D1 the PMTs have a diameter of 5 cm and the expected RMS resolution in front of the PMTs is therefore 2 cm.

#### **Effects on COMPTEL Resolution**

The major determination of the imaging capabilities of COMPTEL is in the spatial resolution of the D1 detector. Tests done on SM II have determined the imaging resolution expected of COMPTEL. From these tests the imaging resolution of the telescope using photons of 5 MeV (1 MeV deposited in D1) was determined to be  $.98^\circ$ . In comparison with the 1 MeV energy range the average spatial resolution as determined by the neural network is 2.31 cm. This value gives the telescope an imaging resolution of  $1.1^\circ$ .

Ten percent of the module has a spatial resolution greater than 3.7 cm with an average value of 5.4 cm. Using this value the imaging resolution of the telescope becomes  $2.1^\circ$ . One of the science questions needed to be addressed is, whether it is acceptable to throw away 10% of the events to maintain the higher imaging resolution or is it necessary to try and reduce these areas of low spatial resolution.

### **Further Development**

The areas of low resolution have shown that questions need to be answered about the signals from events in these areas and the characteristics of the neural network learning. From the resolution and flood test, it is found that events from the edge of the cell between the PMTs seem to have characteristics similar to those in front of the PMTs. These results indicate the neural network can learn from both regions, but locates events only in the regions toward the PMT and central regions. Future work should be done to find the answers to the following questions: Exactly how similar are the signatures of events from regions in front of and between the PMTs? Is there any way to distinguish between events from these two regions? Why is it that the neural network will not locate events along the edge between the PMTs even after learning from them? In answering these question the areas of low spatial resolution may be diminished.

### **Integration of Other Quantities**

One problem the chi squared algorithm faced was that of locating events in the 3-D regions. Results show that the neural network learns to recognize events that have far different signals but correspond to the same location, which is a characteristic of 3-D events. Information about the depth interaction was not needed by the neural network in order for it to locate these types of events. This information, however can easily be integrated in to the network and does not have to be lost as it is now. The process involves changing the input vectors used to teach the neural network by adding the  $\lambda$  value determined from the Principle Component Analysis. The neural network can reproduce the x, y, and  $\lambda$  values for an event in the same way it now produces the x and y values.



## REFERENCES

- Albus, James S., Doctor of Philosophy Dissertation, Theoretical and Experimental Aspects of a Cerebellar Model, University of Maryland, Dec. 1972
- Albus, James S., Mechanisms of Planning and Problem Solving in the Brain, *Mathematical Biosciences*, Vol. 45, 247-293, 1979
- Aleksander, Igor, *Neural Computing Architectures: The Design of Brain-Like Machines*, Cambridge: MIT Press, 1989
- Anger, Hal O., Scintillation Camera, *The Review of Scientific Instruments*, Vol. 29, No. 1, 27-33, Jan. 1958
- Diehl, R., COMPTTEL *Preliminary Design Review Part IV*, MBB Corp., Ottobrunn, W. Germany, Sec. IV.6-Scientific Verification and Calibration, 6, July 10-12, 1984
- Evans, R. D., *The Atomic Nucleus*, New York: McGraw-Hill, 1955
- Franz, J., H. Wolter, K. Manfred, COMPTTEL *Preliminary Design Review Part II*, MBB Corp., Ottobrunn, W. Germany, Sec. II.1-Structure Subsystem, 28, July 10-12, 1984
- Jones, William P., J. Hoskins, Back Propagation, *BYTE Magazine*, 155-162, Oct. 1987
- Kniffen, Donald A., "The Gamma Ray Observatory, Laboratory for High Energy Astrophysics", Reprint, NASA, Goddard Space Flight Center, Dec. 1988
- Lichti, G., COMPTTEL *Preliminary Design Review Part II*, MBB Corp., Ottobrunn, W. Germany, Sec. 4.3 Anticoincidence System, 9, Sept. 21-24, 1982
- Lichti, G., COMPTTEL *Preliminary Design Review Part II*, MBB Corp., Ottobrunn, W. Germany, Sec. II.3 Detector Assembly Subsystem, 6-9, July 10-12, 1984
- Lockwood, J., COMPTTEL *Preliminary Design Review Part II*, MBB Corp., Ottobrunn, W. Germany, Sec. II.2 Detector Assembly Subsystem, 3-4, 29-30, Jul. 10-12, 1984
- McClelland, J. L., J.L. Elman, Chapter 15- Interactive Processes in Speech Perception: The TRACE Model, *Parallel Distributed Processing*, 58-121, Cambridge: MIT Press, 1988
- Miller III, Thomas W., Sensor-Based Control of Robotic Manipulators Using a General Learning Algorithm, *IEEE Journal of Robotics and Automation*, Vol. RA-3, No.2, 157-165, Apr. 1987
- Morris, D., GRO-COMPTTEL-COMPASS Document, Software Requirements for the Module Map Generation Subsystem, Doc. No. COM-SR-UNH-MMG-002, Sept. 1986

- Schönfelder, V., *COMPTEL Preliminary Design Review Part II*, MBB Corp., Ottobrunn, W. Germany, Sec. 1-The Imaging Compton Telescope, 17, Sept 21-24, 1982
- Schönfelder, V., R. Diehl, G. Lichti, H. Steinle, B. Swanenburg, A. Deerenberg, H. Aarts, J. Lockwood, W. Webber, J. Macri, J. Ryan, G. Simpson, B. Taylor, K. Bennet, M. Snelling, *IEEE Trans. Nuc. Sci.*, NS-31(1), 766-770, 1984
- Simpson, G., GRO-COMPTEL-COMPASS Document, SM II D1 Detector Module Spatial Resolution, Doc. No. COM-RP-UNH-F70-014, Apr. 1984
- Simpson, G., GRO-COMPTEL-COMPASS Document, Event-Location using Neural Nets, Doc. No. COM-RP-UNH-F70-038, Nov. 2, 1987a
- Simpson, G., GRO-COMPTEL-COMPASS Document, PMT Resolution From IFC Coefficients, Doc. No. EVP-AL-012-01, Nov. 16, 1987b
- Simpson, G., GRO-COMPTEL-COMPASS Document, Event Location 2D List-Search Algorithm, Doc. No. EVP-AL-003-02, Nov. 17, 1987c
- Steinle, Helmut, GRO-COMPTEL-COMPASS Document, Three Dimensional Event Location With Anger Camera: Application to COMPTEL D2 Module(SM II), Doc. No. COM-TN-MPE-K70-042, Nov. 1985
- Varendorff, M., Three Dimensional Location Resolution of the NaI-Detector used in COMPTEL, Bachelor's Thesis- Technical University of Munich, Mar. 1987
- Zechau, C., *COMPTEL Preliminary Design Review Part II*, MBB Corp., Ottobrunn, W. Germany, Sec. 4.5-Thermal Control Subsystem, 11, Sept 21-24, 1982